UNIVERSITY OF CALIFORNIA, SAN DIEGO

Tectonic and Eustatic Control on Channel Formation, Erosion, and Deposition in the San Diego Bight, CA.

A thesis submitted in partial satisfaction of the requirements for the degree

Master of Science

in

Earth Sciences

by

Lana Genevieve Graves

Committee in charge:

Neal Driscoll, Chair
Alistair Harding
Ed Parnell

2017

The Thesis of Lana Genevieve Graves is approved, and it is acceptable in quality and form for publication on microfilm and electronically:

_____

_____

_____

Chair

University of California, San Diego

2017

DEDICATION

To my dad

EPIGRAPH

The tide goes out imperceptibly. The boulders show and seem to rise up and the ocean recedes leaving little pools, leaving wet weed and moss and sponge, iridescence and brown and blue and China red.

- John Steinbeck

TABLE OF CONTENTS

Signature Page……...iii

Dedication…….....iv

Epigraph……..v

Table of Contents……...vi

List of Figures……...vii

Acknowledgements……..viii

Abstract of the Thesis……ix

1. Introduction……1

2. Methods……...4

3. Results……5
    3.1 Surfaces…….....6
    3.2 Acoustic units……...…….8
    3.3 Faults offsetting the Regional Unconformity……..11
4. Discussion……13
    4.1 The transgressive surface……14
    4.2 Age constraints on observed faulting……..14
    4.3 Extension and subsidence offshore San Diego……...15
    4.4 Eustatic, geologic, and tectonic controls in the San Diego Bight ……..17
    4.5 Tectonic control through the last glacial cycle……...22
    4.6 Available kelp forest substrate and sediment accumulation……...23
5. Conclusion…….....24

6. References…….....27

7. Figures…….....34

LIST OF FIGURES

Figure 1. Maps showing faults, features, and survey lines in the San Diego Bight study area……... 34

Figure 2. Guide to spatial relationship between units (letters) and surfaces (roman numerals)……. 35

Figure 3. Line NH06-L22, uninterpreted (top) and interpreted (bottom)……...……..36

Figure 4a. Line NH06-L18, uninterpreted (top) and interpreted (bottom)……...37

Figure 4b. Line NH06-L41, uninterpreted (top) and interpreted (bottom)……...…38

Figure 5. Line PL15-D02L01, uninterpreted (top) and interpreted (bottom)…….……..39

Figure 6. Line NH06-L58 uninterpreted (top) and interpreted (middle), Line NH06-L24 interpreted (bottom)…….…40

Figure 7. Depth map of Surface I, Surface II, and the Regional Unconformity (RU)……..41

Figure 8. Seismic profiles arranged in 3D fence diagram to provide context for speculated paleochannel locations……..……42

Figure 9. Lines NH06-L7, 9, 11, 13 and 35 intersected by L39, arranged in a fence diagram……..43

Figure 10. Isopach (thickness) maps of Unit C, E, and F…….....44

Figure 11. Figure 11. Fault map of the study area……45

Figure 12. (A) PL15-D01L18, 16, 14, 3, 5, 7, 9, 11 (north to south)……...46

Figure 13. Sea level curves and data referenced in this study……..47

Figure 14. Multichannel Seismic lines interpreted by Maloney (2013).....48

ACKNOWLEDGEMENTS

It has been a privilege to travel over land and sea with Neal Driscoll and learn from him so many lessons of the Earth. I thoroughly enjoyed discussing the data interpretations with Neal, even though it was a bit rough at first, and am thankful for his endless patience and guidance throughout the process. Some lessons have taken a while to stick, but I hope to go forward applying one he told me long ago: 'Do everything with your whole heart and with your whole mind.'

I would like to thank Jillian Maloney for being supportive and for the clarity she brought to this project. I also want to thank my committee members, Alistair Harding and Ed Parnell, for the insights and perspective they thoughtfully imparted.

I'd like to thank Josh Reeves and Sid Eads in the SIO office who have made my transitions through the school's programs very smooth. I also appreciate the work of Monica Bailey, who has been gracious in handling much paperwork for me.

All of my colleagues made my experience in the Driscoll lab such an enjoyable time. I am happy to have shared an office and so many laughs with Emily and James. It has been a real pleasure to share science and the accompanying experiences with Shannon, Boe, Colby, Brendan, Brian, Daniel, Leanne, Mackenzie, and Hector.

I am so grateful to my family for being present and supportive when I have needed them. Bella, I especially appreciate your wisdom. I am grateful to my lab-mate-made-friend, Valerie, for her positive and persistent encouragement. Last but not least, I am thankful for the support and suggestions from Daniel that have acted as an essential catalyst towards completion of this project.

ABSTRACT OF THE THESIS

Tectonic and Eustatic Control on Channel Formation, Erosion, and Deposition in the San Diego Bight, CA.

by

Lana Genevieve Graves

Master of Science in Earth Sciences

University of California, San Diego, 2017

Professor Neal Driscoll, Chair

High-resolution CHIRP seismic surveys were conducted offshore San Diego to understand channel incision, erosion, and deposition throughout a glacial cycle. Eustasy controls deposition and erosion across the local coastal plain and shelf, whereas tectonic deformation controls channel orientation, sediment dispersal pathways, and preservation potential. Sub-parallel, northwest trending fault zones on and offshore San Diego create a structural horst that is bound to the west and east by extensional downdropped faults. The horst creates a bathymetric and topographic high, subaerially expressed as the Point Loma

Peninsula, and is known to be uplifting at the regional rate of ~0.13-0.14 mm/yr. To the east of the bathymetric high, vertical offset along southern splays of the Rose Canyon Fault Zone form a downdropped basin in San Diego Bay and the San Diego Bight. Sediments mantling an MIS 4 erosional surface are interpreted as fluvial and estuarine deposits emplaced during MIS 3. These sediments and underlying units were subsequently truncated and incised during the Last Glacial Maximum (LGM - MIS 2). The preservation of deposits and erosional surfaces is more prevalent to the east of the Southern Spanish Bight Fault. In this region, the Southern Spanish Bight Fault vertically offsets the transgressive surface by an average of ~0.9 m and the interpreted MIS 4 erosional surface by ~4.7 m. Observations of paleo-channelization across the shelf and modern deposition of Holocene sediments indicates that the erosion resistant Cretaceous lithology of the Point Loma Peninsula acts as a drainage divide during periods of low sea level and as a circulation divide during periods of high sea level. The regional tectonic structure, in conjunction with the erosion-resistant character of the local Cretaceous lithology, controls channel architecture, sediment transport and accumulation, as well as nearshore circulation in the San Diego Bight.

1. Introduction

The offshore San Diego region is part of the Inner Continental Borderlands (ICB), which has transitioned from a subduction margin to a strike-slip style margin. The ICB is the western region of the dextral deformation between the Pacific and North American Plate boundary and accommodates ~10-20% of the strain (Bennett, Rodi and Reilinger, 1996; Dixon et al., 2000; Meade and Hager, 2005). The region is transected by several sub-parallel fault zones related to dextral slip along the margin (Bohannon and Geist, 1998; Legg and Kennedy, 1979; Moore and Kennedy, 1975; Ryan et al., 2009; Sahakian et al., 2017; Vedder et al., 1974; Wesnousky, 2005). The southern Newport-Inglewood/Rose Canyon Fault Zone (NIRC) is the major dextral fault system that strikes through the San Diego region and splays have a slip rate of 1-2mm/yr (Figure 1a; Fischer and Mills, 1991; Lindvall and Rockwell, 1995; Moore and Kennedy, 1975). North of the San Diego Bay and Bight, the dextral NIRC makes a left jog inland, creating the transpressional high of Mt. Soledad (Figure 1a; Hogarth et al., 2007; Le Dantec et al., 2010). To the south, geophysical surveys, sediment cores, and offsets along faults in the region reveal that the offshore San Diego Bight and San Diego Bay are part of a subsiding, transtensional basin along a right lateral jog on the NIRC fault system (Kennedy and Clarke, 2001; Kennedy and Welday, 1980; Wiegand, 1970). The most prominent fault splays within this basin are the Spanish Bight, Coronado, and Silver Strand faults (Figure 1a; Gingery et al., 2010; Kennedy and Clarke, 2001; Kennedy and Welday, 1980; Maloney, 2013; Treiman and Lundberg, 1999; Treiman, 2002). Interpretation of multi-channel seismic (MCS) data from offshore also reveal subsidence in San Diego Bay and San Diego Bight relative to the regional uplift of the Point Loma Peninsula (Maloney, 2013). This subsidence has created a sedimentary basin that is bound to the west by the regional

Cretaceous Rosario Group (Kr), expressed as the Point Loma Peninsula and the offshore hardgrounds that anchor the Point Loma kelp forest (Figure 1b; Kennedy and Moore, 1971; Parnell, 2015). Based on marine terraces observed on the peninsula, this relatively erosion resistant Rosario Group is uplifting at the regional rate of ~0.13-0.14mm/yr (Bradley and Griggs, 1976; Kern and Rockwell, 1992; Ku and Kern, 1974; Muhs et al., 2002). This corresponds to the regional southern California uplift rate, which has been purported to be due to rift-flank uplift of the Peninsular Ranges (Mueller et al., 2009). Based on this regional uplift rate and interpretations of deep seismic surveys, Maloney (2013) suggests that the Point Loma Peninsula is not differentially uplifting, but is rather bound by zones of differential subsidence. Fault zones bounding the San Diego Bight include the dextral, east dipping Coronado Bank Fault Zone to the west, the Descanso Fault Zone that is to the west of and subparallel with the Point Loma Peninsula, the west dipping La Nacion Fault Zone to the east, and the dextral San Miguel/Vallecitos Fault Zones to the south (Figure 1a; Artim and Pinckney, 1973; Dixon et al., 2002; Hirabayashi et al., 1996; Maloney, 2013; Ryan et al., 2012).

Sea level fluctuations over the last glacial cycle, from Marine Isotope Stage 5e (MIS 5e, ~125kya) to present, inundated and subaerially exposed the southern California shelf to ~100-120 mbsl (meters below sea level) (Lambeck and Chappell, 2001; Lambeck et al., 2014; Muhs et al., 2012; Reynolds and Simms, 2015; Simms, Rouby and Lambeck, 2016). During early stages of sea level fall, channelized flow extends basinward across the subaerially exposed shelf (Posamentier et al., 1992). In the marine realm, there is a basinward shift in downlap as accommodation decreases. The transition from high to low sea level is marked by the sequence boundary, a surface created by the basinward migration of the shoreline and

subsequent subaerial erosion (Wagoner et al., 1990; Posamentier et al., 1992; Posamentier and Allen, 1999). As sea level falls beyond a shelf break, incised channel valleys form in response to a drop in base level (Wagoner et al., 1990; Posamentier, 2001; Schumm, 1993). During sea level rise, incised channel valleys are filled as the shoreline migrates landward (e.g., Allen and Posamentier, 1993; Thomas and Anderson, 1994; Zaitlin, Dalrymple and Boyd, 1994). The landward migrating shoreline is marked by wave-base erosion, which creates a regional unconformity (the transgressive surface) by eroding shoreface sediments and transporting these both landward and basinward (Christie-Blick and Driscoll, 1995; Posamentier and Allen, 1999). This transgressive surface marks the transition from a subaerial to marine environment (e.g., Allen and Posamentier, 1993; Klotsko et al., 2015; Le Dantec et al., 2010). Periods of slower sea level rise may result in this surface containing better developed abrasion platforms (Bradley and Griggs, 1976). Comparison of regional sea level curves with depths of the transgressive surface yields approximate age-correlated maps of transgression, which may be used to constrain the age of observed faults and features that intersect or overlie the surface.

Once sediment is delivered to the ocean, its transport is controlled by sediment grain size, wave, tidal and current energy, and regional geomorphology. Within the study area, the erosion resistant Cretaceous geology (Rosario Group, Kr) protects the San Diego Bight from north-northwest wave energy (Brownlie and Taylor, 1981; Inman, 1974; Ludka et al., 2015). This results in the net counterclockwise rotation and sediment transport of the Silver Strand Littoral Cell, which is predominantly driven by southern wave energy (Figure 1b; Inman, 1974). It is hypothesized that the Silver Strand, a barrier beach connecting Coronado Island and Imperial Beach, is the result of this littoral transport and slowing rates of sea level rise

over the last ~5-8 kya (Masters, 2006). Modern sediment input to the San Diego Bight is below budget, due to damming within the Tijuana River Valley and other small mountainous rivers that empty into the bay (Converse, 1982; Ellis and Lee, 1919; Inman and Jenkins, 1999; Patsch and Griggs, 2006). As a result, the San Diego Bight is sediment starved and replenishment projects have been pursued to assuage erosion along the Silver Strand (Hein et al., 2003; SANDAG, 2011). Near the northern end of the littoral cell and adjacent to the San Diego Bay entrance is a sediment lobe known as the Zuniga Shoal; this is where the Silver Strand Littoral Cell diminishes in energy and deposits its sediment load (Inman, 1974). Notably, the man-made Zuniga Jetty directly impacts the distribution of the modern Holocene sediments there.

The high resolution CHIRP data presented in this study demonstrate the tectonic control on regional geology, and their conjoined role in sediment accumulation, circulation during sea level highstand, and channel drainage during sea level lowstand.

2. Methods

CHIRP seismic data were collected during cruises in the San Diego Bight from the US-Mexico Border to Point Loma in 2006, 2009, 2015, and 2017 (Figure 1b). The 2006, 2009, and 2015 data were collected with the Scripps Institution of Oceanography EdgeTech X-Star CHIRP sub-bottom reflection sonar towed by the R/V New Horizon, the R/V Robert Gordon Sproul, and the R/V Point Loma, respectively. The frequencies used for these surveys were swept between 1-6 kHz and were transmitted at pulse lengths between 30-50 ms. This swept frequency allows for sub-meter data resolution and subsurface penetration to ~50 m below the sea floor. The instrument was towed between 2-5 m below the sea surface. During a 2017 R/V Sally Ride cruise, subsurface seismic data were collected using the ship's hull-

mounted Knudsen 3260 sub-bottom profiler that transmits dual frequencies of 3.5 kHz and 12 kHz to capture the sub-surface and water bottom depth, respectively. Survey lines parallel to the Silver Strand shoreline (strike lines) and those running perpendicular to it (dip lines) have an average grid spacing of 2 km. The 2006, 2009, and 2015 surveys acquired GPS from the towed system. GPS and navigation were acquired onboard the vessel during the 2017 cruise.

The CHIRP data were collected in EdgeTech's JSF format then converted to SEG-Y format; 2017 data were collected in SEG-Y format. Vessel heave was removed using SeismicUnix (Cohen and Stockwell, 2002) and Sioseis (Henkart, 2003). Identification and interpretation of subsurface horizons and features were performed using IHS Kingdom Suite software (kingdom.ihs.com). QPS Fledermaus software (qps.nl/display/fledermaus) was used for 3D visualization. Maps were created using General Mapping Tools (GMT; gmt.soest.hawaii.edu) and edited in Adobe Illustrator (adobe.com/Illustrator). A grid spacing of 10 m and a spline tension of 0.35 were applied in GMT for interpolation of isopach maps. Geographic data comes from Southern California Coastal Ocean Observing System (sccoos.org/data/bathy; pubs.usgs.gov/sim/2007/2959/) and is projected in NAD83. A nominal velocity of 1500 m/s is used to convert two-way travel time (TWTT) to depth.

3. Results

We observe three surfaces and seven distinct units within the study area, many of which show vertical fault offset. The units vary from west to east and are named according to their interpreted relative age, from oldest to youngest (e.g., A = older, F = younger). Figure 2 presents the relative spatial relationships of the surfaces and units. We will first present the surfaces and their characteristics, followed by the units and descriptions of their acoustic

properties. Lastly, we present the faults observed offsetting the uppermost and youngest surface, which is the Regional Unconformity.

3.1 Surfaces

3.1.1 Surface I

Surface I is characterized as a high relief erosional surface that is observed east of the Rosario Group divide. The depth extent of Surface I is between ~15-45 mbsl, and it appears to deepen subparallel to the modern shoreline (e.g., Figures 3, 4a, 4b, 6, and 7a). The relief on this surface is greater to the north than in the south; however, the amplitude of the reflectivity is greater to the south than in the north (e.g., Figures 6). There is no notable change in character of the surface from east to west. The surface was not identified across the Imperial Beach shoal (Figure 7a).

3.1.2 Surface II

Several concave-up, deeply incising features are observed throughout the eastern survey data and are categorized as Surface II (e.g., Figures 3, 4b, 5, 6, and 7b). In the northeastern Bight, Surface II truncates Surface I. These features are observed incising as deep as ~51 mbsl east of the Rosario Group divide and vary in width from ~500 m to ~2 km (Figure 7b). To the southeast, a deeply incising feature over ~35 m deep is observed directly offshore from the modern, ~2 km wide Tijuana River and estuary complex (Figures 1b and 7b). It is often difficult to ascertain the true depth of Surface II features due to a combination of decreased reflectivity with depth, interference from acoustic ghosts and multiples, and indistinct acoustic character; As a result, the maximum observable depth of reflectors contained within the concave features have been recorded as Surface II (Figure 7b).

In addition to the incised features resembling those observed in Figures 3, 5, and 6, Figure 7b contains the location and depths of features that are concave and increase in depth to the south but do not clearly incise the underlying substrate: These features are shown in Figure 8. In both Figures 8a and 8b, wide, intersecting concave features with maximum observed depths of 46 mbsl and 50 mbsl are observed, respectively. These features contain predominantly transparent fill with faint asymmetric reflectors. Additionally, they are in close proximity to laterally accreted beds observed in Figures 6b and 8b on line NH06 L24. The lateral accreting reflectors are only observed in this area (Figures 6b and 8b), with a marked change in acoustic character away from this region in the other Surface II-like features (e.g., Figure 7). To the south, the concave features are shaded orange in Figure 8b. These features are continuous with Surface I but have been identified as potential Surface II features given their concavity and depth range. In this southeastern region, the underlying units are nearly opaque, precluding confident identification of Surface II. There is a lack of any Surface II features to the west of the well-imaged Rosario Group outcrop (Figure 9).

3.1.3 Regional Unconformity

A regional unconformity (RU) is observed throughout the study area between ~7 to ~95 mbsl (Figures 3, 4a, 4b, 5, 6, 7c, and 9). This RU often truncates underlying reflectors and is mantled by an acoustically transparent deposit in most areas. The acoustic character of the unconformity varies throughout the study region and the changes in reflectivity appear to be influenced by the under- and overlying units (e.g., Figure 4a). The RU forms two abrasion platforms west of the Rosario Group divide. The deeper, west dipping abrasion platform has a bold acoustic reflectivity and dip of ~0.3° and terminates with a marked increase in dip to ~1.1° at ~76 mbsl (Figure 9). The upper abrasion platform has a markedly different acoustic

character than the lower, showing a less amplified reflection with more rugosity, and is observed between ~65 to 53 mbsl, dipping ~0.5° to the west (Figure 9). Towards the east, the RU shoals adjacent to the Rosario Group outcrop, along the Point Loma Peninsula west of the San Diego Bay entrance, and at the Imperial Beach shoal (Figure 7c). This surface also shallows across the San Diego Bight with proximity to the modern shoreline (e.g., Figures 4a, 5, and 7c).

3.2 Acoustic units

3.2.1 Basal units

The Cretaceous Cabrillo, Point Loma, and Lusardi formations are part of the well-mapped Rosario Group (Kr) in the San Diego region (Figures 3, 4a, 4b, and 9; Kennedy and Moore, 1971). As we cannot distinguish between the formations in our seismic survey, we will use Rosario Group in this manuscript when referring to the Cretaceous deposits in the study area. In this region, the Rosario Group is identifiable by its east dipping reflectors and outcrop relief. It has been incorporated into a north-northwest striking anticline in the extensional hanging wall of the Coronado Bank Fault (Figure 9; Maloney, 2013). Figure 4a reveals that the eastern limb of this anticline forms a seafloor outcrop of the Rosario Group that effectively divides the study area into western and eastern regions, where distinct acoustic units and surfaces are observed on either side (e.g., Figures 2 and 4a).

To the west of the anticline, clearly imaged southwest dipping beds are observed extending to the shelf edge at ~100 mbsl (Figures 1b and 9). These have a true dip between 2° and 5° to the southwest and collectively are identified as Unit A (e.g., Figure 4a and 9). The lower (deeper) abrasion platform truncates the underlying reflectors of Unit A (Figures 4a and 9).

The features observed in the eastern Bight, that are truncated or underlying all surfaces are considered components of Unit B. Adjacent to and overlying the eastern Rosario Group, this unit contains (true) northwest to southwest dipping reflectors (Figures 3 and 4b). Towards the east, Unit B contains true west dipping reflectors (Figure 6b). To the south below Surfaces I and II, no notable features are apparent in Unit B (Figure 6a).

3.2.2 Infilling units

Overlying Surface I to the northeast is Unit C (e.g., Figures 3, 4a, 6, and 10a). This unit is acoustically transparent to chaotic and infills Surface I relief (e.g., Figure 3). South and east of the Imperial Beach shoal, Unit C exhibits discontinuous reflectors that diminish with distance from the Tijuana River Valley (Figure 6a). This unit has a maximum observed thickness of less than 5 m and pinches out adjacent to the Rosario Group outcrop. Surface II clearly truncates Unit C (e.g., Figures 3 and 5).

This infill of the incised and concave Surface II features is categorized as Unit D, and the locations of this unit are the same as Surface II observations (e.g., Figures 3, 4b, 5, 6, and 7b). Several of the northeastern Surface II incised features are filled with a sequence of depositional units: The lowest is a blotchy to transparent unit, the middle deposit features laminations with a thickness of ~1 m or less that onlap or abut Surface II, and the uppermost is a transparent to chaotic deposit overlying a shallow, concave erosional unconformity (e.g., Figures 3, 5, 6a, and 10b). The southeastern concave features do not contain this characteristic sequence and instead are infilled with acoustically transparent to chaotic fill (Figure 8b). In Figure 7b, the locations of stratified Unit D observations are outlined in black to delineate them from those without stratification. Near the center of the eastern study area laterally

accreting reflectors are observed to the east and adjacent to a Surface II observation (Line NH06 L24, Figures 6b and 8b).

3.2.3 Modern units

Two acoustic units are observed above the RU (Figures 4a, 9, 10c, and 10d). Along the western escarpment of the Rosario Group outcrop, the RU is covered by acoustic Unit E that exhibits high amplitude, discontinuous reflectors (Figures 4a, 9, and 10c). The areal extent of Unit E is limited, being only observed in close proximity to the west and south of the Rosario Group outcrop. Additionally, the western limit of Unit E is spatially coincident with the increase in dip of the RU between the upper and lower platforms. Unit E thickens to the south, reaching a maximum thickness of ~4.5 m at the southern limit of coverage, precluding additional thickness estimates (Figure 9).

Overlying Unit E is an acoustically transparent deposit, Unit F. This unit is observed blanketing much of the study area (e.g., Figures 3, 4a, 4b, 5, 6, and 10d). To the west of the Rosario Group hardgrounds, Unit F pinches out before the shelf edge and is thickest where the RU increases in slope west of the lower abrasion platform (Figure 9 and 10d). East of the Rosario Group outcrop, Unit F mantles much of the study area (e.g., Figure 4a). The thickness of Unit F varies markedly throughout the study region ranging from ~9 m at its depocenter on the Zuniga Shoal to less than a meter across the eastern edge of the Rosario Group deposits (Figures 4a, 4b, 9, and 10d). Unit F cover diminishes to the south and becomes thin (<1m) or absent with proximity to the shoreline (e.g., Figures 3, 5, and 10d). Additionally, Unit F appears to be absent over the Imperial Beach shoal; however, there might be a thin veneer of sediment below the CHIRP vertical resolution or obscured by dense kelp coverage during the time of data collection (Figures 1b and 10d). There is a lobe of Unit F located offshore from

the Tijuana River near the US-Mexico border (Figure 10d) with thicknesses on the order of ~3m. A few faint discontinuous reflectors are observed within the unit.

3.3 Faults offsetting the Regional Unconformity

3.3.1 Silver Strand Fault

The Silver Strand Fault trends northeast – southwest in the study area. Nonetheless, it is observed intersecting survey line PL15-D02L01, which also trends north-south (Figures 5 and 11). In this region, there is an observed minor left jog in the Silver Strand Fault based on previous mapping, which may explain the intersection (Figure 11). In line PL15-D02L01, the fault offsets dipping and rotated strata in the south from flat lying to slightly diverging strata to the north. The RU is offset by 0.75 m across the fault (Figure 5). The deeper reflectors may record larger cumulative offset (~10 m); however, there is uncertainty correlating reflectors across the fault. The fault offset is south of an incised Surface II feature proximal to the onshore Otay River and north of the Imperial Beach shoal (Figures 5 and 11).

3.3.2 Southern Spanish Bight Fault

East of the Rosario Group outcrop, a ~6 km long, northeast trending lineation of vertical offsets of the RU are observed, with a down to east component of deformation (e.g., Figures 3, 4a, and 11). The traced RU offset lies to the south of, and equidistantly between, the mapped Spanish Bight and Coronado faults, and here will be referred to as the Southern Spanish Bight Fault (SSB, Figure 11). The extent of vertical offset across the RU ranges from 0.75 to 0.94 m between ~24-34 mbsl. Where the SSB Fault intersects Surface I, at least ~4.7 m of displacement is observed (e.g., Figures 3 and 7a). Additionally, Unit C is thickest east of the SSB Fault (Figure 10a). The overlying Unit F shows no evidence of displacement (e.g.,

Figures 3 and 4a); however, there are few if any reflectors observed in this unit to record deformation and offset. To the south, Unit B is blotchy to acoustically opaque, inhibiting observation of any SSB Fault offset within it (e.g., Figures 6a and 8b).

3.3.3 Point Loma Fault Zone

Within the eastern Rosario Group geology observed offshore Point Loma, strata appear to have been tectonically deformed or displaced with a down to the east dip-slip component of deformation within in the Point Loma Fault Zone (Figure 12). South of Point Loma, it is difficult to ascertain if the RU has been offset adjacent to the Rosario Group outcrop because of its faint acoustic character in this region, possibly due to the thick overlying sediment (e.g., Figures 4a, 4b, and 12b). However, along the eastern side of the Point Loma promontory and extending north into the bay, minor displacements of the RU and deformation of the Rosario Group strata are observed (Figure 12a). The survey lines near the bay entrance image a buried abrasion platform with minor offset along distributed faults (Figure 12a). Complexity the fault zone and the features it intersects increases with proximity to Ballast Point to the north as additional reflectors are imaged and the planar nature of the RU changes (Figure 12a). As can be observed in Figure 12a, cross sections F, G, and H have multiple high amplitude reflectors above the RU. In lines A, B, C, and D of Figure 12a, the change in slope of the RU is spatially coincident with the mapped trace of the Point Loma Fault, which strikes approximately due north in this region (Figure 1a and 11).

3.3.4 Descanso Fault Zone

The upper abrasion platform of the RU is vertically offset by faults spatially correlated to the previously mapped Descanso Fault Zone (DFZ) (Figures 1a, 9, and 11). These offsets

are minimal in the north and increase to ~1 to 2 m towards the south (e.g., Figure 9). The lack of continuous internal reflectors within the overlying Unit E makes it difficult to determine if there has been fault activity along since its deposition. Notably, the lower (deeper) abrasion platform of the RU, which is to the west of the observed DFZ offsets, shows no vertical offset and there is little internal deformation of the underlying Unit A (Figure 9).

4. Discussion

We will first discuss the interpretation of the RU and its implications for timing of observed fault offsets. This will be followed by a discussion of the tectonic structure offshore San Diego. Finally, we will interpret the observed offshore features and deposits in the context of tectonic deformation and sea level change throughout the last glacial cycle.

To assess the timing of features observed in the San Diego Bight, we compare the depths of these features to the global maximum and minimum sea level curves. In Figure 13, we present the sea level curves of Lambeck and Chappell (2001) and Lambeck et al. (2014), which account for glacial isostatic adjustment (GIA), together with the non-GIA incorporated global sea level curve of Lea et al. (2003). Additionally, the data compiled by Reynolds and Simms (2015) from several physical indicators of sea level during the Holocene, and the modeled GIA influenced local sea level curve of Muhs et al. (2012), are overlain on the sea level curves since the last glacial maximum (MIS 2) and since the last sea level highstand (MIS 5e; Figure 13). This compilation of curves is presented to demonstrate that, despite being far from centers of glacial growth, the role of glacial isostatic adjustment (GIA) has been considered in southern California (see discussion in Muhs et al., 2012). GIA calculations are sensitive to both the ice and earth models they are based on and yield different amplitudes of sea level fluctuations (Farrell and Clark, 1976; Khan et al., 2015; Lambeck and Nakada,

1985; Muhs et al., 2012; Nakada and Lambeck, 1989; Potter and Lambeck, 2004; Tamisiea, 2011). We employ the sea level curves to constrain times when accommodation is created or destroyed and to impose an upper age limit on observed fault offsets.

4.1 The transgressive surface

The shoreline and associated wave base erosion migrate landward when sea level rise outpaces sediment supply and uplift (Christie-Blick and Driscoll, 1995; Posamentier and Vail, 1988). As sea level rises, this wave base erosion results in an unconformity, referred to as the transgressive surface (e.g., Klotsko et al., 2015; Le Dantec et al., 2010). We interpret the RU to be the transgressive surface associated with the rise in sea level following MIS 2 (Figures 7d and 13). Comparing the depths of the RU with the sea level curves from Muhs et al. (2012) and Lambeck et al. (2014; Figure 13), we approximate the timing of shoreline transgression, which places relative age constraints on observed features in the study area.

4.2 Age constraints on observed faulting

The main fault strands observed in this study that offset the transgressive surface (i.e., the RU) are delineated in Figure 11. Offsets of the transgressive surface by the SSB Fault are observed between depths of ~24-34 mbsl. The shoreline transgressed this depth range between ~8-10 kya (Figure 13; Lambeck et al., 2014; Muhs et al., 2012). The Silver Strand Fault offset is observed at ~15 mbsl that corresponds to a maximum age range of ~7-8.5 kya (Figures 5 and 13). Additionally, the slightly diverging reflectors that terminate against this fault and the folding and deformation south of the fault suggest it has been active prior to the transgression (Figure 5). The transgressive surface appears offset and deformed by the Point Loma Fault Zone suggesting post transgression activity in water depths of ~10 m, ~6-8 kya at

the bay mouth (Figures 11, 12, and 13). Vertical offsets of the RU in discontinuous locations are observed within the mapped Descanso Fault Zone (Figure 9). This suggests the most recent dip-slip displacement on this fault zone postdates ~10-12 kya, when the shoreline transgressed the region between ~65-40 mbsl (Figures 11 and 13).

4.3 Extension and Subsidence offshore San Diego

The San Diego Bay and Bight are within a region of extension and subsidence associated with a right jog in the dextral NIRC fault system (Figure 1a; Darigo and Osborne, 1986; Kennedy and Welday, 1980; Maloney, 2013; Moore and Kennedy, 1975). Onshore, long-term subsidence is evidenced by a negative gravity anomaly that increases seaward, indicating the presence of lower density deposits west of the La Nacion Fault Zone, inferred to result from extensive basin sediment fill (Figures 1a; Marshall, 1997). Observations of over 120 m of vertical offset in Pleistocene deposits west of the La Nacion Fault Zone and seismic profiles within the bay that record over 150 m of Pleistocene sediments appear to represent only a fraction of the filled accommodation that has been created through subsidence (Artim and Pinckney, 1973; Kennedy and Clarke, 2001). Evidence of Holocene extension and subsidence in the San Diego region include ~1 m of down to the west displacement of Holocene sediments across the La Nacion Fault Zone, displaced sediments dated to ~4.4 kya along the Silver Strand Fault in San Diego Bay, and offset of ~0.29 m along the Coronado Fault constrained by soil development to within the last few hundred years (Artim and Pinckney, 1973; Gingery et al., 2010; Kennedy and Clarke, 2001). While Kennedy and Clarke (2001) report that across the northern section of bay, the Spanish Bight, Coronado, and Silver Strand faults all dip primarily to the east with a normal component, they assess that the easternmost strand of the Silver Strand Fault dips nearly vertical with down to the west

displacement (Figure 1a and 11). Kennedy and Clarke (2001) suggest that the axis of the extensional graben lies between the easternmost and westernmost components of the Silver Strand Fault mapped in the Bay (Figure 11; Fault D1 of Kennedy and Clarke, 2001). Additionally, Kennedy and Clarke (2001) suggest that this down-to-the-west fault strand crosses the Silver Strand barrier beach into the San Diego Bight. The extent of subsidence to the south and east of the bay is unclear; dating of the reported Tijuana Terrace and the relatively elevated onshore extension of the Imperial Beach Shoal may provide further insight (Artim and Pinckney, 1973; Ellis and Lee, 1919; Kern, 1977).

Presented in Figure 14 are MCS lines interpreted by Maloney (2013) that image the subsurface to depths of ~1.5 km between the San Diego coastline and the Coronado Bank Faults (Figure 11). Imaged in these lines is extension accommodated by rollover along the Coronado Bank Fault Zone and down to the west, dip-slip displacement along the Descanso Fault Zone. In Figure 14b, the west dipping Descanso Fault Zone and east dipping Spanish Bight Fault create the Point Loma Horst bound by extensional, sediment-filled basins to the west and east (Maloney, 2013). The upper component of the horst is interpreted to be the Cretaceous Rosario Group, which is present in the landward, subaerially exposed Point Loma Peninsula (Figures 11 and 14) and in seafloor outcrops offshore from the peninsula. As the Point Loma horst block and associated peninsula is uplifting at a rate of ~0.13-0.14 mm/yr, which is within the range of regional terrace uplift, we interpret the observed relief as being the result of differential subsidence, not differential uplift (Kern and Rockwell, 1992; Maloney, 2013; Mueller et al., 2009). It can be observed in Figure 14c that the relief on the horst block dies away to the south; the seismic signature of Cretaceous rock may be present at greater depths but it appears that the two basins observed in Figure 14b are conjoined.

While we cannot calculate the rate of subsidence within the downdropped basin between the Point Loma horst block and the La Nacion Fault Zone or eastern Silver Strand splays, subsidence has preserved Pleistocene deposits throughout the Quaternary glacial cycles (Kennedy and Clarke, 2001). The rate of subsidence in the San Diego Bay and Bight is therefore necessarily equal to or greater than the regional uplift rate, given this long-term creation of accommodation.

4.4 Eustatic, geologic, and tectonic controls in the San Diego Bight

4.4.1 Sediment supply throughout the glacial cycle

To understand the evolution of the Bight throughout the glacial cycle in the context of local subsidence, it is important to assess sediment supply to the area. In the absence of prominent sandstone sea cliffs, the main source of sediment in the study area is from local rivers (Inman, 1974; Olsen et al., 2016; Young et al., 2010). Channels feeding into the San Diego Bay and Bight originate in the Peninsular Ranges at elevations between 1000 and 3000 m and have drainage basins less than 10 km^2 (Brownlie and Taylor, 1981; Ellis and Lee, 1919; Inman 1974). These channels do not have wide flood plains and reach the shoreline within ~13 km from their origin, with the exception of the Tijuana River which extends over ~80 km inland (Ellis and Lee, 1919). Given these characteristics, the regional channels may be classified as small, mountainous rivers (Hogarth, 2010; Milliman and Syvitski, 1992). Hogarth (2010) determined that the sediment load from these rivers to the shelf is consistent throughout the glacial cycle, contrasting with broad alluvial plain rivers that deliver punctuated amounts of stored sediment during rapid falls in base level. We assume that sediment delivery to the shelf is roughly constant throughout the glacial cycle with the

exception of the sea level low stand, when incised channels transport increased amounts of sediment load to the slope (Hogarth, 2010; Posamentier and Vail, 1988).

4.4.2 Units interpreted to predate the Last Interglacial

Observed west of the Rosario Group and below the transgressive surface, the west dipping beds of Unit A have been interpreted to predate the Last Interglacial and are prograding clinoforms of Miocene to late Pleistocene age (Emery et al., 1952; Kennedy and Welday, 1980; Vedder et al., 1974). Darigo and Osborne (1986) interpreted Unit B, located east of the Rosario Group outcrop, to range in age from the Eocene to the Pliocene based on onshore geological relationships (Kennedy et al., 1975; Kennedy and Welday, 1980). Situated below Surface I and incised by Surface II, Unit B could have been deposited anytime before MIS 4 when Surface I is interpreted to have been formed. This interpretation is consistent with differential subsidence increasing to the east (Maloney, 2013); It is likely that the more eastern components of Unit B are younger than those adjacent to the Rosario Group geology in the west (Darigo and Osborne, 1986).

4.4.3 Eustatic and geologic control: Last Interglacial to the Last Glacial Maximum

We interpret erosional Surface I to be a subaerially formed erosion surface corresponding to the time period of or following the MIS 4 sea level fall to ~65-85 mbsl (Figures 7a and 13; Christie-Blick and Driscoll, 1995). Land above ~50 mbsl exposed during MIS 4 was not resubmerged until the MIS 1 transgression (Figure 13). Surface I is only observed between ~15-45 mbsl, but may have extended to greater depths that were subsequently reworked by wave-base erosion during MIS 3. The high relief character of Surface I suggests subaerial erosion, likely fluvial in nature. The response of fluvial systems

to changes in base level is dependent on many factors, particularly the slope of a newly exposed surface, the rate of base level change, and the depth of the shelf slope break (Anderson et al., 2004; Posamentier et al., 1992; Schumm, 1993; Törnqvist et al., 2006). During MIS 4 the fall in sea level did not extend past the shelf edge, which is ~100-120 mbsl in the study area (Figures 1 and 13). Given the sea level fall exposed only the shelf without a significant increase in slope, fluvial downcutting and incision would have been minor (Posamentier, 2001; Schumm, 1993; Törnqvist et al., 2006). Nevertheless, cores from the Coronado Canyon contain evidence that there was off-shelf transport of sediments from the Tijuana River during MIS 4, suggesting that the Coronado Canyon head (~60 mbsl), which is about 15 km from the modern coast, was near the shoreline at this time (Dartnell et al., 2007; Normark et al., 2009).

Overlying Surface I in the northeastern San Diego Bight is Unit C, which we interpret to be the subaerial deposit formed following the erosion of Surface I, possibly during the intermediate sea level rise of MIS 3 (Figures 10a and 13). A change in base level adjusts the slope crossed by a fluvial system, allowing for aggradation or erosion along their profiles and/or a change in sinuosity to maintain equilibrium (Posamentier et al., 1992; Schumm, 1993). When the fluvial profile shallows, as with base level rise, aggradation and increased channel sinuosity ensue (Schumm, 1993). The infilling of Surface I high relief character by Unit C suggests new subaerial accommodation had been created for sediment deposition in regions ranging from ~15–45 mbsl (Figure 3, 4a, 13).

The incised features of Surface II that truncate the MIS 3 deposit (Unit C) and MIS 4 erosional surface (Surface I) are interpreted to be components the sequence boundary created by fluvial incision during sea level fall of MIS 2 (Figures 7b and 13; Anderson et al., 2004;

Christie-Blick and Driscoll, 1995; Törnqvist et al., 2006). Globally, sea level is assessed to have reached about ~120 mbsl (Fairbanks, 1989). However, due to locational differences in GIA, it has been suggested that the San Diego region experienced a maximum sea level low between 95-100 mbsl (Muhs et al., 2012; Simms, Rouby and Lambeck, 2015). Nonetheless, while the shelf edge in the study area is at or greater than this depth, the head of the Coronado Canyon is less than 65-85 mbsl, and this shelf break would have been exposed for several thousand years. As incision may occur when sea level falls below a break in slope and the channel system erodes to establish a new equilibrium profile (Posamentier et al., 1992; Posamentier, 2001; Schumm, 1993), the Coronado Canyon head likely served as this shelf break to initiate incision on the shelf during MIS 2. Dated sediments from the Coronado Canyon indicate that it was connected with the Tijuana River during MIS 4 and MIS 2 (Dartnell et al., 2007; Normark et al., 2009); Channels of the northern San Diego Bight may have joined the Tijuana River to the south as tributaries or directly connected to the Coronado Canyon during these times. While the complete route of paleochannels from source to sink remains obscure (Figure 7b), the absence of incised channels along western boundary of the study area and the absence of significant sediment inputs to the Loma Sea Valley during MIS 2 suggests the channels were deflected south by the outcropping Rosario Group hardgrounds during the most recent glacial cycle (Figure 7b; Covault et al., 2007). We suggest that the erosion resistant Rosario Group geology, in combination with the sediment filled down-dropping basin to its east, funneled the fluvial discharge south during the MIS 2 sea level fall (Figure 7b).

4.4.4 Eustatic control: Last Glacial Maximum to present

The channel fill (Unit D) in our interpretation began to aggrade following the MIS 2 low stand (Figure 13). The stratified infill observed in many of the incised channel features reveals a shallowing pattern associated with transgression in fluvial channels on a low-gradient continental shelf environment (e.g., Figures 3, 4b, and 5; e.g., Thomas and Anderson et al., 1994; Zaitlin, Dalrymple and Boyd, 1994). The bottommost unit exhibits an acoustically transparent to blotchy character and is interpreted to be fluvial, deposited following the LGM (e.g., Figures 3 and 5). The horizontal laminations of the middle unit onlap the channel walls and may record a transition from fluvial to estuarine deposits as relative seal level continued to rise creating new accommodation. The uppermost unit is acoustically transparent to chaotic in nature and is often observed above a scour surface (e.g., Figure 3), which may be the result of nearshore tidal scour and subsequent infilling (Posamentier and Allen, 1999); this upper most unit may correspond to the Type II Holocene deposit reported by Darigo and Osborne (1986) that contained chaotically oriented and alternating marine and nonmarine sediments located within the bounds of drowned channel valleys. The localized laterally accreting beds that are observed in the central channel region (Figures 6b and 8b) are interpreted as a point bar deposit in the fluvial system. The channel feature adjacent to the point bar deposit (Figures 6b and 8b) is infilled by an acoustically transparent unit that does not resemble the more stratified channel fill observed to the north and east as seen in Figures 3 and 5 . We interpret that this predominantly transparent channel fill was deposited after the channelized flow that produced the localized point bar deposit.

Overlying the transgressive surface are Units E and F. Based on its high amplitude acoustic character and prograding nature, Unit E is interpreted to be a transgressive lag associated with erosion of the shallower regions across the Rosario Group outcrops during the

subsequent sea level rise that shunted coarse material seaward. The local distribution of Unit E just west of the outcropping Rosario Group hardgrounds may reflect the limited mobility of this transgressive lag due to its inferred coarser grain size content. Unit F is modern sediment that accumulated with the slow in sea level of the last ~10 kyr, which corresponds to the findings of previous studies (Darigo and Osborne, 1986; Emery et al., 1952; Inman, 1974).

The depths of the lower abrasion platform of the transgressive surface is observed between ~76-90 mbsl, corresponds to shoreline transgression between ~16-13 kya and is at similar water depths as a studied terrace west of San Clemente Island (Figures 9 and 13; Derosier et al., 2015; Lambeck et al., 2014; Muhs et al., 2012). The upper abrasion platform, observed between ~65 to 53 mbsl, is closer to the depths of regional platforms attributed to the slow down in the rate of sea level rise associated with the Younger Dryas (e.g., Figure 13; Klotsko et al., 2015). We interpret the increased slope of the RU between the lower and upper abrasion platforms to be a shoreline angle. There is marked increase in the thickness of the Holocene sediment (Unit F) in the area of the shoreline angle (Figures 9 and 10d). Unit E is present east of the shoreline angle and over the upper platform (Figures 9 and 10c).

4.5 Tectonic control throughout the last glacial cycle

The role of tectonics in the study area may be divided into two components: 1) differential subsidence exposing an erosion resistant geology that acts as a physical divide during both low and high sea levels, and 2) transtensional subsidence that creates accommodation and preserves stratigraphic features. As noted, the southeast trending Rosario Group outcrop south of Point Loma forms a drainage divide during lowstand conditions and redirects drainage systems toward the south (Figure 7c). This juxtaposition of the erosion resistant horst with the eastern sediment basin is directly related to the regional tectonics

(Figures 11 and 14). The outcropping Rosario Group hardgrounds also control sediment thickness and dispersal during higher sea levels; this is consistent with the different Holocene sediment characteristics observed on the sea floor on either side of the outcrop (Figure 7b; Emery et al., 1952). Note the large thickness of Holocene sediment infilling the accommodation along the southern end of Zuniga Jetty as a result of the counter-clockwise circulation in the region; the Silver Strand Littoral Cell is controlled in part by northern wave energy sheltering of the Point Loma Peninsula (Figure 1b).

Subsidence driven accommodation is observed in the slight increase in Holocene sediment thickness across the SSB Fault (Figures 3, 4a, and 10d). Additionally, down to the east offset of this fault corresponds to a deepening of the erosional surface (Surface I) and maximum thickness of the overlying deposit (Unit C; Figures 3, 7a, and 10a). It is inferred that subsidence preceding the MIS 1 transgression along the SSB Fault increased the preservation potential of the MIS 4 erosional surface and MIS 3 deposit by lowering them below the depth of wave base erosion associated with shoreline transgression (Posamentier and Allen, 1999).

4.6 Available kelp forest substrate and sediment accumulation

The role of the exposed erosion-resistant Rosario Group geological unit offshore San Diego as a geophysical and biological systems parameter has long been appreciated (Converse, 1982; Inman, 1974; Kennedy and Moore, 1971). This exposed, tectonically controlled geological unit provides a hard substrate for kelp anchorage and deflects wave energy from the north and west, thereby influencing circulation and sediment transport in the San Diego Bight (Figure 1a; Emery et al., 1952; Inman, 1974). The holdfasts of Macrocystis pyrifera, foundational kelp forest species offshore southern California, requires stable

substrate for anchorage; a few centimeters of sediment coverage does not affect established algae; however, it inhibits the anchoring of juvenile organisms (Dayton, 1985; Devinny and Volse, 1978; Parnell et al., 2006). While additional factors such as substrate rugosity and persistent sea urchin barrens strongly influence kelp forest concentration, understanding the rate of uplift relative to the adjacent sediment basin of the Bight will provide insight into the available substrate of the future as it has been shown that tectonically forced habitats influence species abundance and diversity patterns in the marine environment (Maloney, 2013; Parnell, 2015; Switzer et al., 2015). In our data set, we observe that vertical throw of the SSB Fault creates minor accommodation for sediments transported to the midshelf by the Silver Strand Littoral Cell (e.g., Figures 1a, 3, and 4a). This accommodation does not offset the accumulation of the littorally transported and San Diego Bay sourced sediments at the Zuniga Shoal, to the north of the SSB Fault. While the ~9 m depocenter of the shoal is ~2 km from the current extent of kelp forest substrate, the mound's margins already encroach ~500 m onto the eastern Rosario Group within the habitable depth range of <~35 mbsl (e.g., Figure 4a; Dayton, 1985; Maloney, 2013; Parnell et al., 2006). If sea level continues to rise at the current rate of ~1 to 3 mm/yr, continued longshore transport of sands from the erodible Silver Strand barrier beach and Coronado Island may bury portions of the outcropping Rosario Group hardgrounds and threaten kelp substrate availability (IPCC, 2013; Maloney, 2013; Reynolds and Simms, 2015).

5. Conclusion

Analysis of high resolution CHIRP data collected in the San Diego Bight provided age constraints for recent fault activity and demonstrated the control of eustasy and regional tectonics on channelization, circulation and sedimentation.

1. All observed faults appear Holocene active based on timing of sea-level transgression and offset of the transgressive surface. Observations of fault offsets in this study, in conjunction with the findings of previous research, indicate the region offshore San Diego is a transtensional basin connected to a more southerly extensional basin bounded to the west by the Coronado Bank Fault Zone.
2. Differential subsidence in the region appears to control preservation of sediment deposited prior to the most recent sea-level transgression. Subsidence to the east of the SSB Fault has increased the preservation potential of the erosional surface formed during or following the sea level fall of MIS 4 (Surface I) and the overlying unit interpreted to be emplaced during MIS 3 when sea level rose across the region (Unit C).
3. Regional tectonics juxtapose erosion resistant Cretaceous geology offshore Point Loma with the subsiding basin to the east, which help control sediment dispersal in the Bight during times of both low and high sea-level. During falling and low sea levels, the Cretaceous outcrop and extensional faulting to the east divert channel systems to the south. During high sea levels, outcropping Cretaceous hardgrounds provide minimal accommodation for modern sediment deposition, while the promontory deflects northwest wave energy allowing deposition in the continuously subsiding basin that engenders accommodation. In contrast, the southern region of the San Diego Bight is exposed to southern wave energy and is nearly sediment bare.

Incorporation of the fault offsets and their age constraints recorded here augment understanding of tectonic activity in the San Diego and Southern California region. In the future, core collection throughout the Bight will help establish a chronostratigraphic

framework for the region. Additional seismic surveys to the south of the study area across the US – Mexican border will further elucidate the regional channel network.

6. References

Allen, G.P. and Posamentier, H.W., 1993. Sequence stratigraphy and facies model of an incised valley fill: the Gironde estuary, France. *Journal of Sedimentary Research*, 63(3), 378–391.

Anderson, J.B., Rodriquez, A., Abdulah, K.C., Fillon, R.H., Banfield, L.A., Mckeown, H.A., and Wellner, J.S., 2004. Late Quaternary stratigraphic evolution of the northern Gulf of Mexico margin: a synthesis. *SEPM Special Publication No. 79*, 1–23.

Artim, E.R. and Pinckney, C.J., 1973. La Nación Fault System, San Diego, California. *Geological Society of America Bulletin*, 84(3), 1075–1080.

Basile, C. and Brun, J.P., 1999. Transtensional faulting patterns ranging from pull-apart basins to transform continental margins: An experimental investigation. *Journal of Structural Geology*, 21(1), 23–37.

Bennett, R.A., Rodi, W. and Reilinger, R.E., 1996. Global Positioning System constraints on fault slip rates in southern California and northern Baja, Mexico. *Journal of Geophysical Research: Solid Earth*, 101(B10), 21943–21960.

Bohannon, R.G. and Geist, E., 1998. Upper crustal structure and Neogene tectonic development of the California continental borderland. *Geological Society of America Bulletin*, 110(6), 779–800.

Bradley, W.C. and Griggs, G.B., 1976. Form, genesis, and deformation of central California wave-cut platforms. *Geological Society of America Bulletin*, 87(3), 433–449.

Brownlie, W.R. and Taylor, B.D., 1981. *Sediment Management for Southern California Mountains, Coastal Plains, and Shoreline; Part C: Coastal Sediment Delivery by Major Rivers in Southern California*. Pasadena, California: California Institute of Technology, *EQL Report No. 17-C,* 314p.

Christie-Blick, N. and Driscoll, N.W., 1995. Sequence stratigraphy. *Annual Review of Earth and Planetary Sciences*, 23(1), 451–478.

Cohen, J.K. and Stockwell Jr., J.W., 1999. CWP/SU: Seismic Unix Release 33: a free package for seismic research and process, software. Center for Wave Phenomena, Colorado School of Mines, Golden, CO.

Converse, H., 1982. Barrier beach features of California. *Coastal Engineering 1982*, 1008–1027.

Covault, J.A., Normark, W.R., Romans, B.W. and Graham, S.A., 2007. Highstand fans in the California borderland: The overlooked deep-water depositional systems. *Geology*, 35(9), 783–786.

Cunningham, D., 2007. Structural and topographic characteristics of restraining bend mountain ranges of the Altai, Gobi Altai and easternmost Tien Shan. *Geological Society, London, Special Publications*, 290(1), 219–237.

Darigo, N.J. and Osborne, R.H., 1986. Quaternary stratigraphy and sedimentation of the inner continental shelf, San Diego County, California. *Canadian Society of Petroleum Geologists, Memoir II: Shelf Sands and Sandstones*, 73–98.

Darntell, P., Normark, W.R, Driscoll, N.W., Babcock, J.M., Gardner, J.V., Kvitek, R.G. and

Iampietro, P., 2007. *Multibeam bathymetry and selected perspective views offshore San Diego, California*: U.S. Geological Survey Scientific Investigations Map 2959, 2 sheets. http://pubs.usgs.gov/sim/2007/2959.

Dayton, P.K., 1985. Ecology of kelp communities. *Annual review of ecology and systematics, 16(1),* pp. 215-345.

Derosier, B., Driscoll, N.W., Graves, L.G., Holmes, J.J. and Nicholson, C., 2015. New CHIRP seismic images of Submarine Terraces around San Clemente Island constrain its tectonic evolution and geomorphology. *AGU Fall Meeting 2015,* abstract #T51A-2847.

Devinny, J.S. and Volse, L.A., 1978. Effects of sediments on the development of Macrocystis pyrifera gametophytes. *Marine biology*, 48(4), 343–348.

Dixon, T., Farina, F., DeMets, C., Suarez-Vidal, F., Fletcher, J., Marques-Azua, B., Miller, M., Sanchez, O. and Umhoefer, P., 2000. New kinematic models for Pacific-North America Motion from 3 Ma to Present, II: Evidence for a "Baja California Shear Zone." *Geophysical Research Letters*, 27(23), 3961–3964.

Dixon, T., Decaix, J., Farina, F., Furlong, K., Malservisi, R., Bennet, R., Suarez-Vidal, F., Fletcher, J. and Lee, J., 2002. Seismic cycle and rheological effects on estimation of present-day slip rates for the Agua Blanca and San Miguel-Vallecitos faults, northern Baja California, Mexico. *Journal of Geophysical Research*, 107(B10), 1-23.

Ellis, A.J. and Lee, C., 1919. Geology and ground waters of the western part of San Diego County, California. *US Geological Survey Water Supply Paper 446*, 321p.

Emery, K.O., Butcher, W.S., Gould, H.R. and Shepard, F.P., 1952. Submarine Geology off San Diego, California. *The Journal of Geology*, 60(6), 511–548.

Fairbanks, R.G., 1989. A 17,000-year glacio-eustatic sea level record: influence of glacial melting rates on the Younger Dryas event and deep-ocean circulation. *Nature*, 342(6250), 637–642.

Farrell, W.E. and Clark, J.A., 1976. On postglacial sea level. *Geophysical Journal International*, 46(3), 647–667.

Fischer, P.J. and Mills, G.I., 1991. The offshore Newport-Inglewood\Rose Canyon Fault Zone, California: Structure, segmentation, and tectonics. In *Environmental Perils, San Diego Region. San Diego Association of Geologists for Geologic Society of America Meeting*. 17–36.

Gingery, J.R., Rugg, S.H., Rochwell, T.K. and Hilton, B.R., 2010. Fault Hazard Characterization for a Transportation Tunnel Project in Coronado, California*. Fifth International Conference on Recent Advances in Geotechnical Earthquake Engineering and Soil Dynamics* (San Diego, California, 24 May 2010), *Paper No. 7.02c*. 13p.

Hein, J.R., Dowling, J.S, Schuetze, A. and Homa, J.L., 2003. Clay-mineral suites, sources, and inferred dispersal routes: Southern California continental shelf. *Marine Environmental Research*, 56(1–2), 79–102.

Henkart, P., 2003. SIOSEIS, software. Scripps Institution of Oceanography, La Jolla, CA. http://sioseis.ucsd.edu.

Hirabayashi, C.K., Rockwell, T.K., Wesnousky, S.G., Stirling, M.W. and Suarez-Vidal, F., 1996. A

neotectonic study of the San Miguel-Vallecitos Fault, Baja California, Mexico. *Bulletin of the Seismological Society of America*, 86(6), 1770–1783.

Hogarth, L.J., Babcock, J., Driscoll, N.W., Le Dantec, N., Haas, J.K., Inman, D.L. and Masters, P.M., 2007. Long-term tectonic control on Holocene shelf sedimentation offshore La Jolla, California. *Geology*, 35(3), 275–278.

Hogarth, L.J., 2010. Tectonic Signatures on Active Margins. San Diego, California: University of California San Diego, Ph.D. dissertation, 121p.

Inman, D.L., 1974. *Nearshore processes along the Silver Strand littoral cell*. La Jolla, California: Intersea Research Corporation, 15 Aug. 1974.

Inman, D.L. and Jenkins, S.A., 1999. Climate change and the episodicity of sediment flux of small California rivers. *The Journal of Geology*, 107(3), 251–270.

Kennedy, M.P. and Moore, G.W., 1971. Stratigraphic relations of upper Cretaceous and Eocene formations, San Diego coastal area, California. *American Association of Petroleum Geologists Bulletin*, 55(5), 709–722.

Kennedy, M.P., 1975. Geology of the San Diego Metropolitan Area, California: Del Mar, La Jolla, and Point Loma quadrangles. *California Division of Mines and Geology Bulletin*, 200, 39p.

Kennedy, M.P. and Welday, E.E., 1980. *Recency and Character of Faulting Offshore Metropolitan San Diego, California (Area 3 of 3)*, California Division of Mines and Geology, Map Sheet 42.

Kennedy, M.P. and Clarke, S.H., 2001. Late Quaternary faulting in San Diego Bay and hazard to the Coronado Bridge. *California Geology*, 54(4), 4–17.

Kern, J.P., 1977. Origin and history of upper Pleistocene marine terraces, San Diego, California. *Geological Society of America Bulletin*, 88(11), 1553–1566.

Kern, J.P. and Rockwell, T.K., 1992. Chronology and deformation of Quaternary marine shorelines, San Diego county, California. *Quaternary Coasts of the U.S.: Marine and Lacustrine Systems*, 377–382.

Khan, N.S., Ashe, E., Shaw, T.A., Vacchi, M., Walker, J., Peltier, W.R., Kopp, R.E. and Horton, B.P., 2015. Holocene Relative Sea-Level Changes from Near-, Intermediate-, and Far-Field Locations. *Current Climate Change Reports*, 1(4), 247–262.

Klotsko, S., Driscoll, N.W., Kent, G. and Brothers, D., 2015. Continental shelf morphology and stratigraphy offshore San Onofre, California: The interplay between rates of eustatic change and sediment supply. *Marine Geology*, 369, 116–126.

Ku, T.-L. and Kern, J.P., 1974. Uranium-series age of the upper Pleistocene Nestor terrace, San Diego, California. *Geological Society of America Bulletin*, 85(11), 1713–1716.

Lambeck, K. and Nakada, M., 1985. Holocene fluctuations in sea level: constraints on mantle viscosity and melt-water sources. *Proceedings of the Fifth International Coral Reef Congress, Tahiti*, *3,* pp. 79–84.

Lambeck, K. and Chappell, J., 2001. Sea Level Change Through the Last Glacial Cycle. *Science*, 292(5517), 679–686.

Lambeck, K., Rouby, H., Purcell, A., Sun, Y. and Sambridge, M., 2014. Sea level and global ice volumes from the Last Glacial Maximum to the Holocene. *Proceedings of the National Academy of Sciences of the United States of America*, 111(43), 15296–303.

Le Dantec, N., Hogarth, L.J., Driscoll, N.W., Babcock, J.M., Barnhardt, W.A. and Schwab, W.C., 2010. Tectonic controls on nearshore sediment accumulation and submarine canyon morphology offshore La Jolla , Southern California. *Marine Geology*, 268(1–4), 115–128.

Lea, D.W., Martin, P.A., Pak, D.K. and Spero, H.J., 2002. Reconstructing a 350 ky history of sea level using planktonic Mg/Ca and oxygen isotope records from a Cocos Ridge core. *Quaternary Science Reviews*, 21(1–3), 283–293.

Legg, M.R. and Kennedy, M.P., 1979. Faulting offshore San Diego and northern Baja California. *In:* Abbott, P.L. and Elliott, W.J. (eds.), *Earthquakes and other perils - San Diego Region, Geological Society of America Annual Meeting Guidebook* (San Diego, California), pp. 29–46.

Lindvall, S.C. and Rockwell, T.K., 1995. Holocene activity of the Rose Canyon Fault Zone in San Diego, California. *Journal of Geophysical Research: Solid Earth*, 100(B12), 24121–24132.

Ludka, B.C., Guza, R.T., O'Reilly, W.C. and Yates, M.L., 2015. Field evidence of beach profile evolution toward equilibrium. *Journal of Geophysical Research: Oceans*, 120(11), 7574–7597.

Maloney, J., 2013. Fault Segments and Step-overs: Implications for Geohazards and Biohabitats. San Diego, California: University of California San Diego, Ph.D. disseration, 210p.

Marshall, M., 1997. Detailed Gravity Studies and the Tectonics of the Rose Canyon – Point Loma – La Nación Fault System, San Diego, California. *In:* Roquemore, G. (ed.), *The Seismic Risk in the San Diego Region: Special Focus on the Rose Canyon Fault Systems: Workshop Proceedings* (San Diego, California), pp. 80-100.

Masters, P.M., 2006. Holocene sand beaches of southern California: ENSO forcing and coastal processes on millennial scales. *Palaeogeography, Palaeoclimatology, Palaeoecology*, 232(1), 73–95.

MBC Applied Environmental Sciences Staff, 2016. *Status of the kelp beds in 2015: Ventura, Los Angeles, Orange, and San Diego Counties. Central Region Kelp Survey Consortium and Region Nine Kelp Survey Consortium.* Costa Mesa, California: MBC Applied Environmental Sciences, 71p.

Meade, B.J. and Hager, B.H., 2005. Block models of crustal motion in southern California constrained by GPS measurements. *Journal of Geophysical Research: Solid Earth*, 110(B3), 1-19.

Milliman, J.D. and Syvitski, J.P.M., 1992. Geomorphic/tectonic control of sediment discharge to the ocean: the importance of small mountainous rivers. *The Journal of Geology*, 100(5), 525–544.

Moore, G.W. and Kennedy, M.P., 1975. Quaternary faults at San Diego Bay, California. *Journal of Research US Geological Survey,* 3(5), 589–595.

Mueller, K., Kier, G., Rockwell, T. and Jones, C.H., 2009. Quaternary rift flank uplift of the Peninsular Ranges in Baja and southern California by removal of mantle lithosphere. *Tectonics*, 28(5), 1–17.

Muhs, D.R., Simmons, K.R., Kennedy, G.L. and Rockwell, T.K., 2002. The last interglacial period on

the pacific coast of north america:timing and paleoclimate. *Geological Society of America Bulletin*, (5), 569–592.

Muhs, D.R., Simmons, K.R., Schumann, R.R., Groves, L.T., Mitrovica, J.X. and Laurel, D., 2012. Sea-level history during the Last Interglacial complex on San Nicolas Island, California: Implications for glacial isostatic adjustment processes, paleozoogeography and tectonics. *Quaternary Science Reviews*, 37, 1–25.

Nakada, M. and Lambeck, K., 1989. Late Pleistocene and Holocene sea-level change in the Australian region and mantle rheology. *Geophysical Journal International*, 96(3), 497–517.

Normark, W.R., Piper, D.J.W., Romans, B.W., Covault, J.A., Dartnell, P. and Sliter, R.W., 2009. Submarine canyon and fan systems of the California Continental Borderland. *In:* Lee, H.J. and Normark W.R. (eds.), *Earth Science in the Urban Ocean: The Southern California Continental Borderland: Geological Society of America Special Paper 454*, pp. 141–168.

Olsen, M.J., Johnstone, E., Driscoll, N.W., Kuester, F. and Ashford, S.A., 2016. Fate and transport of seacliff failure sediment in southern California. *Journal of Coastal Research,* 76(sp1), 185-199.

Parnell, P.E., Dayton, P.K., Lennert-Cody, C.E., Rasmussen, L.L. and Leichter, J.J., 2006. Marine reserve design: Optimal size, habitats, species affinities, diversity, and ocean microclimate. *Ecological Applications*, 16(3), 945–962.

Parnell, P.E., 2015. The effects of seascape pattern on algal patch structure, sea urchin barrens, and ecological processes. *Journal of Experimental Marine Biology and Ecology*, 465, 64–76.

Patsch, K. and Griggs, G., 2006. *Littoral cells, sand budgets, and beaches: understanding California's shoreline*. Santa Cruz, California: Institute of Marine Sciences, University of California, Santa Cruz. 40p.

Posamentier, H.W. and Vail, P.R., 1988. Eustatic controls on clastic deposition II—sequence and systems tract models. *SEPM Special Publication,* No. 42, 125-154.

Posamentier, H.W., Allen, G.P., James, D.P. and Tesson, M., 1992. Forced regressions in a sequence stratigraphic framework: concepts, examples, and exploration significance. *American Association of Petroleum Geologists Bulletin*, 76(11), 1687–1709.

Posamentier, H.W. and Allen, G.P., 1999. *Siliciclastic sequence stratigraphy: concepts and applications*, Tulsa, Arizona: Society for Sedimentary Geology, 210p.

Posamentier, H.W., 2001. Lowstand alluvial bypass systems: Incised vs. unincised. *American Association of Petroleum Geologists Bulletin*, 85(10), 1771–1793.

Potter, E.K. and Lambeck, K., 2004. Reconciliation of sea-level observations in the Western North Atlantic during the last glacial cycle. *Earth and Planetary Science Letters*, 217(1–2), 171–181.

Reynolds, L.C. and Simms, A.R., 2015. Late Quaternary relative sea level in Southern California and Monterey Bay. *Quaternary Science Reviews*, 126, 57–66.

Ryan, H.F., Legg, M.R., Conrad, J.E. and Sliter, R.W., 2009. Recent faulting in the Gulf of Santa Catalina : San Diego to Dana Point. *The Geological Society of America. Special Paper 454*, 291–315.

Ryan, H.F., Conrad, J.E., Paull, C.K. and McGann, M., 2012. Slip rate on the San Diego Trough Fault Zone, Inner California Borderland, and the 1986 Oceanside earthquake swarm revisited. *Bulletin of the Seismological Society of America*, 102(6), 2300–2312.

Sahakian, V., Bormann, J., Driscoll, N.W., Harding, A., Kent, G. and Wesnousky, S., 2017. Seismic constraints on the architecture of the Newport-Inglewood/Rose Canyon fault: Implications for the length and magnitude of future earthquake ruptures. *Journal of Geophysical Research: Solid Earth*, 122(3), 2085–2105.

SANDAG, 2011. *Final Environmental Impact Report (Revised) for the San Diego Regional Beach Sand Project II.* San Diego Associatation of Governments (SANDAG), State Clearinghouse Number 2010051063, 622p.

Schumm, S.A., 1993. River Response to Baselevel Change : Implications for Sequence Stratigraphy. *The Journal of Geology*, 101(2), 279–294.

Simms, A.R., Rouby, H. and Lambeck, K., 2016. Marine terraces and rates of vertical tectonic motion: The importance of glacio-isostatic adjustment along the Pacific coast of central North America. *Bulletin of the Geological Society of America*, 128(1–2), 81–93.

Switzer, R.D., Parnell, P.E., Leichter, J.L. and Driscoll, N.W., 2016. The effects of tectonic deformation and sediment allocation on shelf habitats and megabenthic distribution and diversity in southern California. *Estuarine, Coastal, and Shelf Science*, 169, 25–37.

Tamisiea, M.E., 2011. The Moving boundaries of Sea Level Change. *Oceanography*, 24(Sea Level), 24–39.

Thomas, M.A. and Anderson, J.B., 1994. Sea-level controls on the facies architecture of the Trinity/Sabine incised-valley system, Texas continental shelf. *SEPM Special Publication* No. 15, 63-82.

Törnqvist, T.E., Wortman, S.R., Mateo, Z.R.P., Milne, G.A. and Swenson, J.B., 2006. Did the last sea level lowstand always lead to cross-shelf valley formation and source-to-sink sediment flux? *Journal of Geophysical Research: Earth Surface*, 111(4), 1–13.

Treiman, J.A. and Lundberg, M., compilers, 1999. Fault number 127g, *Newport-Inglewood-Rose Canyon Fault Zone, Silver Strand section. In: Quaternary fault and fold database of the United States, U.S. Geological Survey website,* https://earthquakes.usgs.gov/hazards/qfaults.

Treiman, J., 2002. *Silver Strand Fault, Coronado Fault, Spanish Bight Fault, San Diego Fault, and Downtown Graben, Southern Rose Canyon Fault Zone, San Diego, California*. *California Division of Mines and Geology Fault Evaluation Report FER-245,* 25p.

U.S. Geological Survey, 2012. *Quaternary fold and fault database of the United States*. https://earthquake.usgs.gov/hazards/qfaults/kml.php

Van Wagoner, J.C., Mitchum, R.M., Campion, K.M. and Rahmanian, V.D., 1990. *Siliciclastic sequence stratigraphy in well logs, cores, and outcrops: concepts for high-resolution correlation of time and facies,* Tulsa, Oklahoma: AAPG Methods in Exploration Series, No. 7, 55p.

Vedder, J.G., Beyer, L.A., Junger, A., Moore, G.W., Roberts, A.E., Tayler, J.C. and Wagner, H.C., 1974. *Preliminary report on the geology of the Continental Borderland of southern California*,

US Geological Survey, 14p.

Wesnousky, S.G., 2005. The San Andreas and Walker Lane Fault Systems, western North America: Transpression, transtension, cumulative slip and the structural evolution of a major transform plate boundary. *Journal of Structural Geology*, 27(8), 1505–1512.

Wiegand, J.W., 1970. Evidence of a San Diego Bay-Tijuana fault. *Bulletin of the Association of Engineering Geologists*, 7, 107–121.

Woodcock, N.H. and Fischer, M., 1986. Strike-slip duplexes. *Journal of structural geology*, 8(7), 725–735.

Wu, J.E., McClay, K., Whitehouse, P. and Dooley, T., 2009. 4D analogue modelling of transtensional pull-apart basins. *Marine and Petroleum Geology*, 26(8), 1608–1623.

Young, A.P., Raymond, J.H., Sorenson, J., Johnstone, E.A., Driscoll, N.W., Flick, R.E. and Guza, R.T., 2010. Coarse Sediment Yields from Seacliff Erosion in the Oceanside Littoral Cell. *Journal of Coastal Research*, 263(263), 580–585.

Zaitlin, B.A., Dalrymple, R.W. and Boyd, R.O.N., 1994. The stratigraphic organization of incised-valley systems associated with relative sea-level change. *SEPM Special Publication*, No. 51, 45–60.

7. Figures

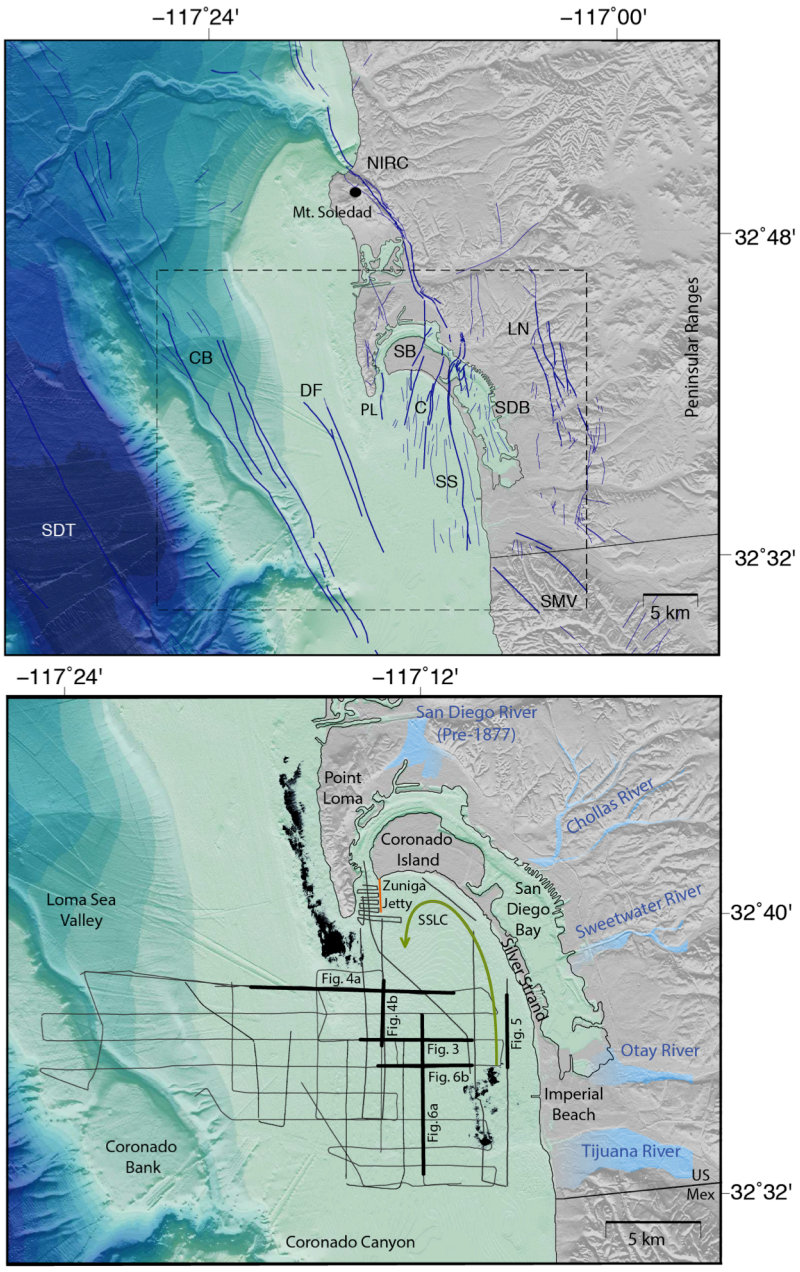

Figure 1. Maps showing faults, features, and survey lines in the San Diego Bight study area. Regional maps of onshore and offshore San Diego, CA, with bathymetry modified from Dartnell et al. (2007). (A) Regional faults (USGS, 2012) transecting the San Diego Bight and surrounding area are shown in blue. Dashed box indicates location of Figure 1b. SDT= San Diego Trough Fault Zone; CB = Coronado Bank Fault Zone; DF = Descanso Fault Zone; SB = Spanish Bight Fault; C = Coronado Fault; SS = Silver Strand Fault; PL = Point Loma Fault Zone; SDB = San Diego Bay Fault Zone (which include the SB, C, and SS faults); NIRC = Newport-Inglewood/Rose Canyon Fault Zone; LN = La Nacion Fault Zone; SMV = San Miguel/Vallecitos Fault Zone. (B) Map of containing the nearshore San Diego Bight, showing seismic survey track lines analyzed in this study. Kelp data from 2015 (MBC, 2016) colored in black. Silver Strand Littoral Cell (SSLC) counterclockwise circulation pattern shown in green.

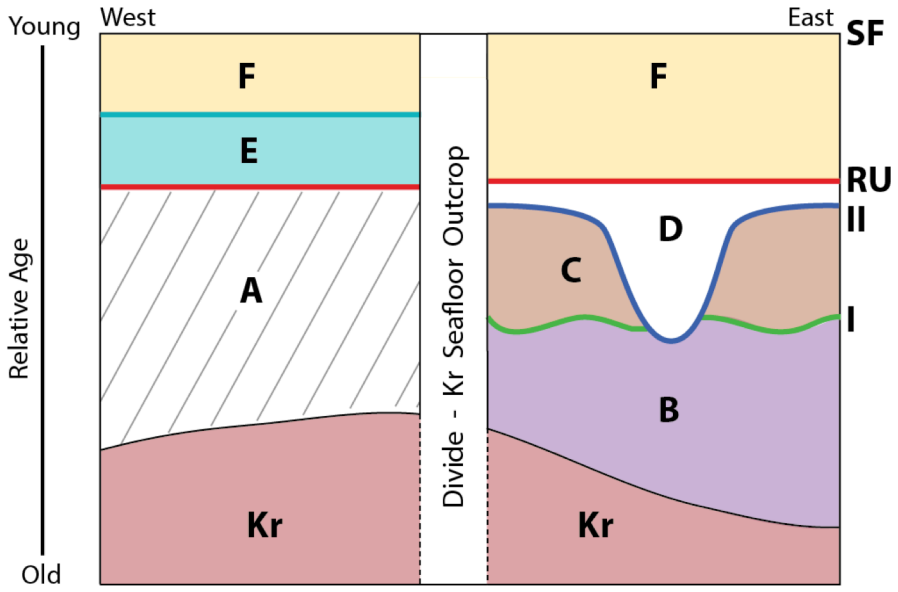

Figure 2. Guide to spatial relationship between units (letters) and surfaces (roman numerals). Columns are arranged by spatial (west to east) and relative age (old to young) relationships. The Kr seafloor outcrop creates the divide between the two columns. Note the relative age relationships are not correlated across the Kr divide. RU = Regional unconformity; SF = Sea floor.

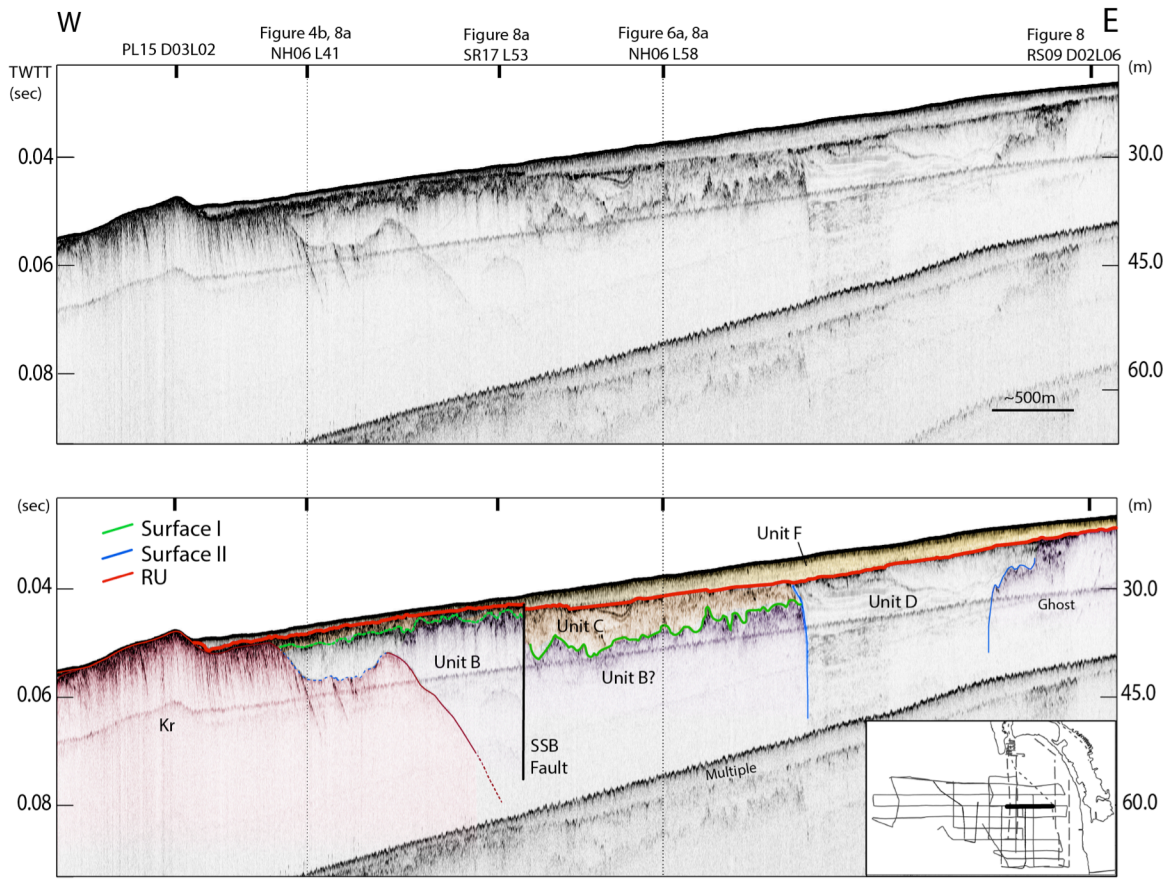

Figure 3. Line NH06-L22, uninterpreted (top) and interpreted (bottom). Inset shows location on map of this line (black). Perpendicular to Figure 6a, this profile shows the relationship between the Cretaceous (Kr) rock and adjacent units. The Southern Spanish Bight (SSB) Fault is observed offsetting the RU and Surface I.

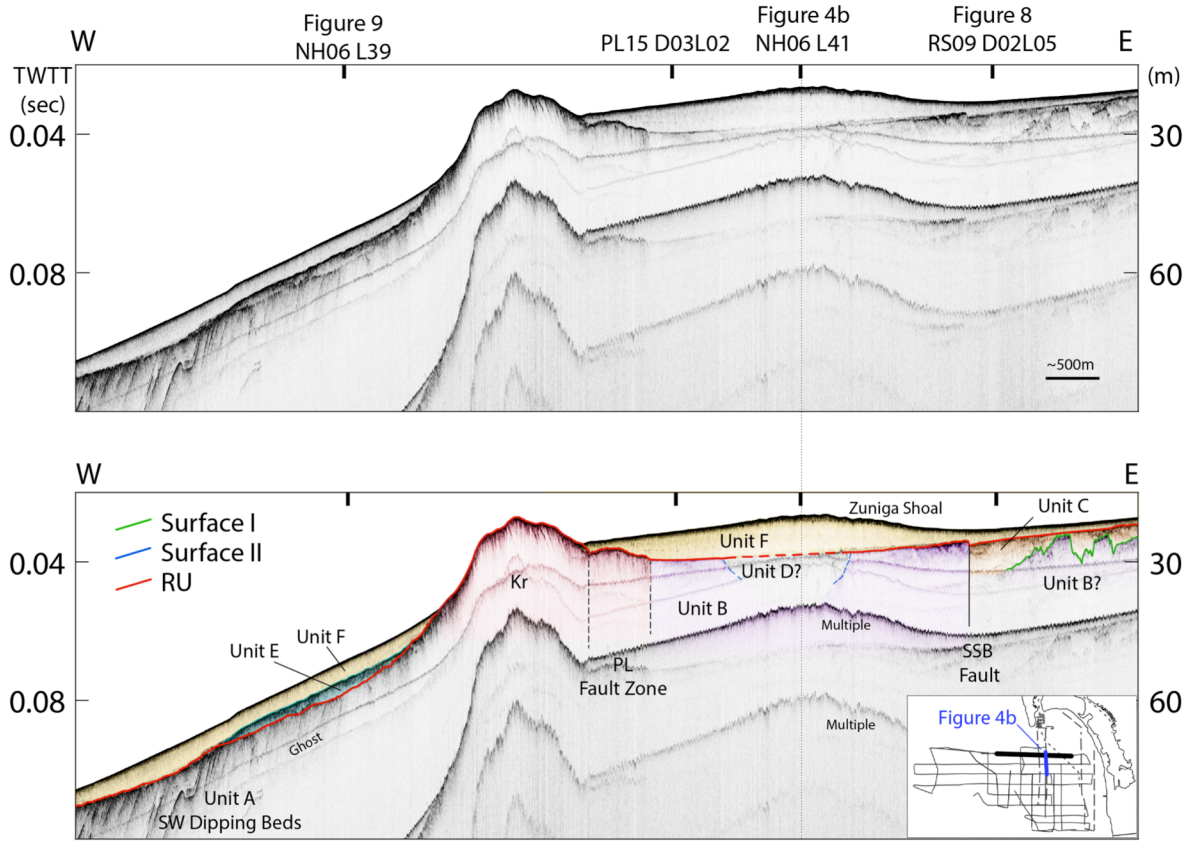

Figure 4a. Line NH06-L18, uninterpreted (top) and interpreted (bottom). Inset shows location on map of this line (black) and Figure 4b (blue). The Cretaceous Rosario Group (Kr) outcrop is composed of the eastern limb of a north-northwest trending anticline and exhibits east-dipping beds. Unit A, composed of west dipping beds, is present to the west of the Kr outcrop. Unit B is adjacent to the Kr geology, although its extent is uncertain: see Figure 4b for observations of dipping reflectors within Unit B. Units E and F overlie the Regional Unconformity (RU); Unit F is observed throughout much of the study area. The Zuniga shoal can be observed to the east of the Kr outcrop. Surface I, a high relief erosional surface, separates Unit B from Unit C. The trough-like channel trace of Surface II is inferred from intersecting profiles (see Figure 4b). PL = Point Loma; SSB = Southern Spanish Bight.

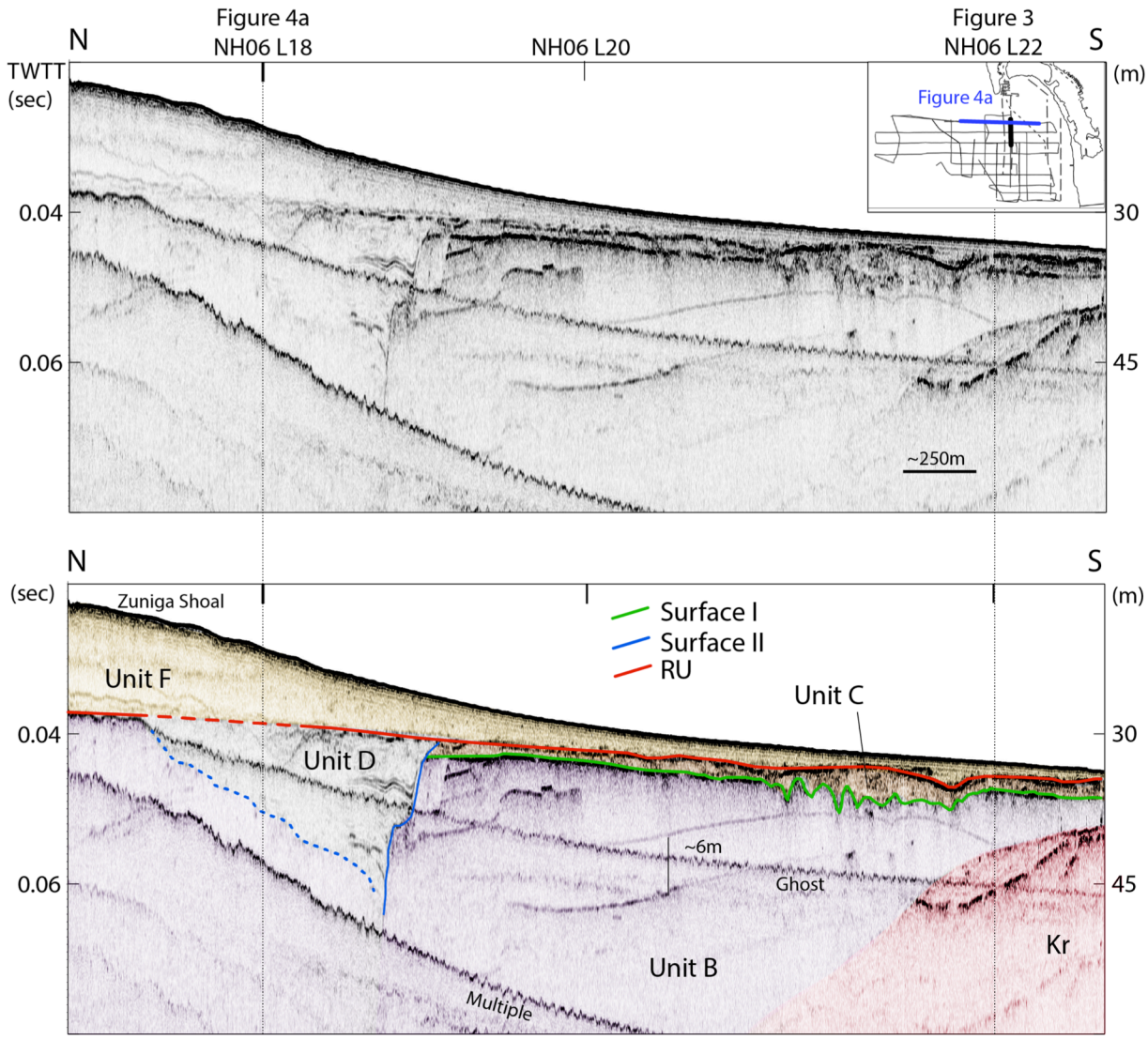

Figure 4b. Line NH06-L41, uninterpreted (top) and interpreted (bottom). Inset shows location on map of this line (black) and Figure 4a (blue). See Figure 4a caption for unit and surface relationships. Notably, this profile shows the dipping beds of Unit B: these appear to dip north in cross section, but perpendicular lines show the dip of these reflectors changes from northwest in the north to southwest in the south. Additionally, Surface I here separates Unit B below from Unit C above. Surface II traces the channel-like feature observed here and inferred in Figure 4a. RU = regional unconformity.

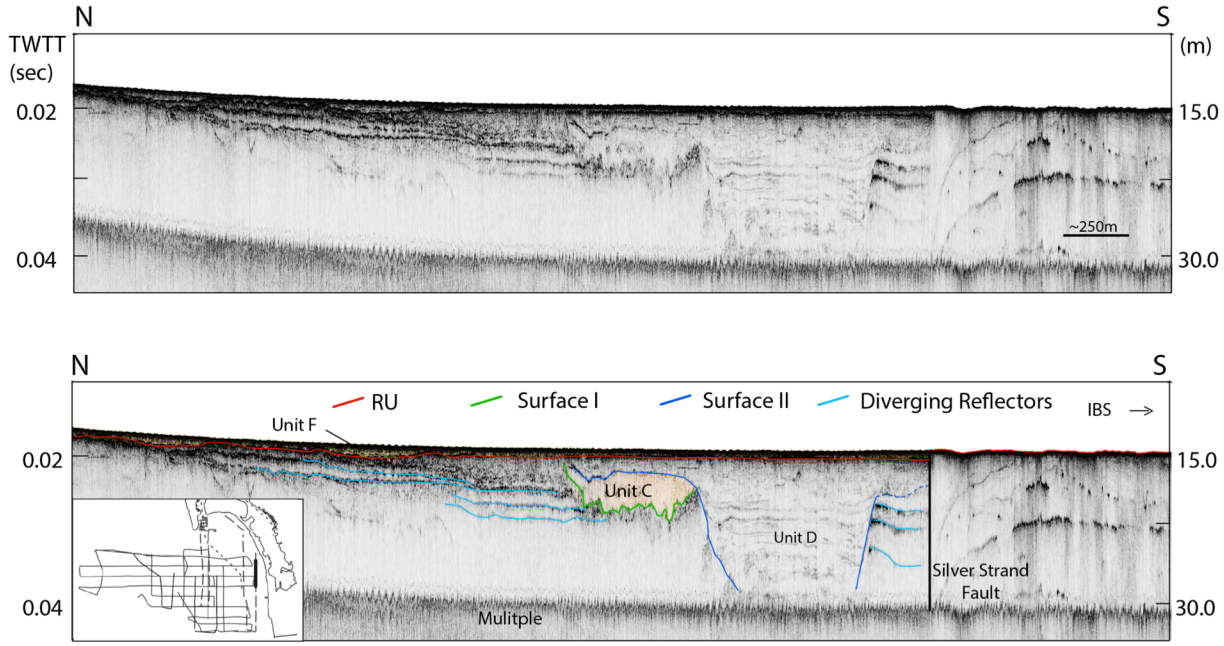

Figure 5. Line PL15-D02L01, uninterpreted (top) and interpreted (bottom). Inset shows location of line traced in thick black. The Regional unconformity (RU) shoals nearshore and Unit F has thinned. Profile shows offset and reflector terminations by the Silver Strand Fault (see Figure 1a). Fault offset is to the south of the channel feature and to the north of the Imperial Beach Shoal (IBS, see Figure 1).

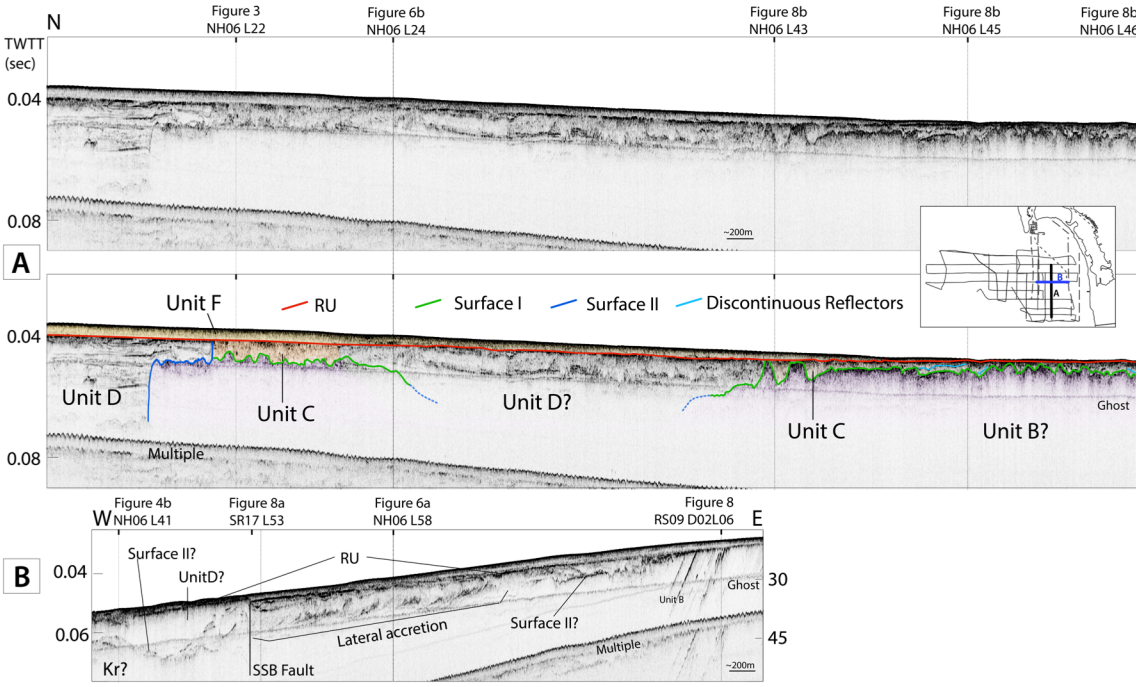

Figure 6. Line NH06-L58 uninterpreted (top) and interpreted (middle), Line NH06-L24 interpreted (bottom). (A) Line NH06-L58 inset shows location of Figures 6a traced in thick black and Figure 6b traced in blue. The north to south survey line shows the differing character of Surfaces I and II, and the units that are below and above these. Note the dashed Surface II trace near the center of the survey is inferred from cross section with line NH06-L24 in Figure 6b, which shows laterally accreting reflectors. RU = regional unconformity. (B) Line NH06-24.

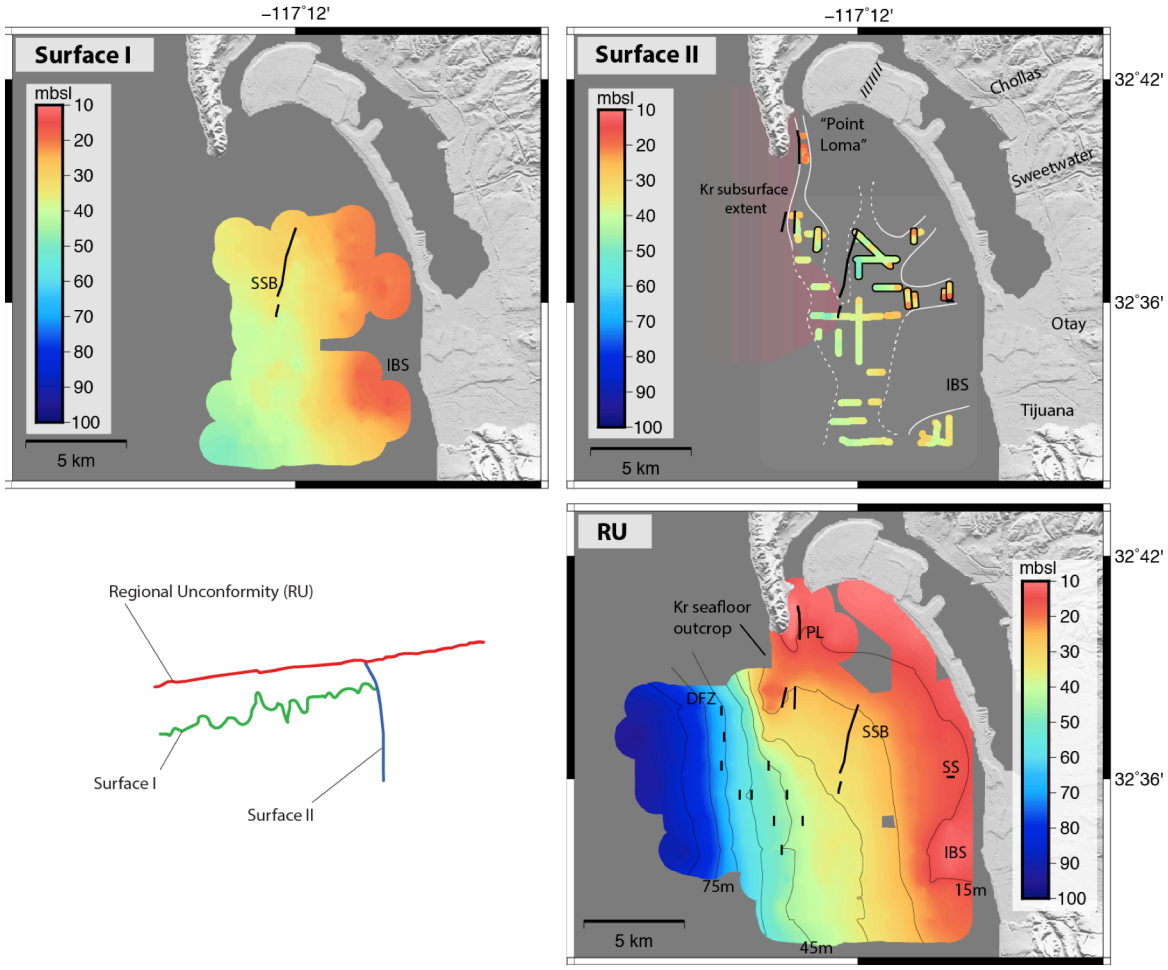

Figure 7. Depth map of Surface I, Surface II, and the Regional Unconformity (RU). (A) Depth map of Surface I. SSB = Southern Spanish Bight Fault; IBS = Imperial Beach Shoal. (B) Depth map of Surface II features. The depths represent the deepest observed reflectors, note incision may have extended to greater depths. The observed subsurface extent of the Cretaceous (Kr) geology is represented in magenta. Modern, onshore rivers are labeled. Outlined in white is the inferred MIS 2 channel route: dashed white indicates where there is uncertainty regarding channel location (see discussion). Outlined in black are locations where Surface II is filled with the sequential chaotic-laminated-transparent fill sequence of Unit D. (C) Schematic showing cross-cutting relationships of surfaces. (D) Depth map of the Regional Unconformity (RU). The Kr seafloor outcrop and the Imperial Beach Shoal (IBS) are identifiable as anomalously shallowing features. Overlain on the RU are contours with 10m spacing and faults observed in this study that offset the RU: DFZ = Descanso Fault Zone; SSB = Southern Spanish Bight Fault; PL = Point Loma Fault Zone; SS = Silver Strand Fault.

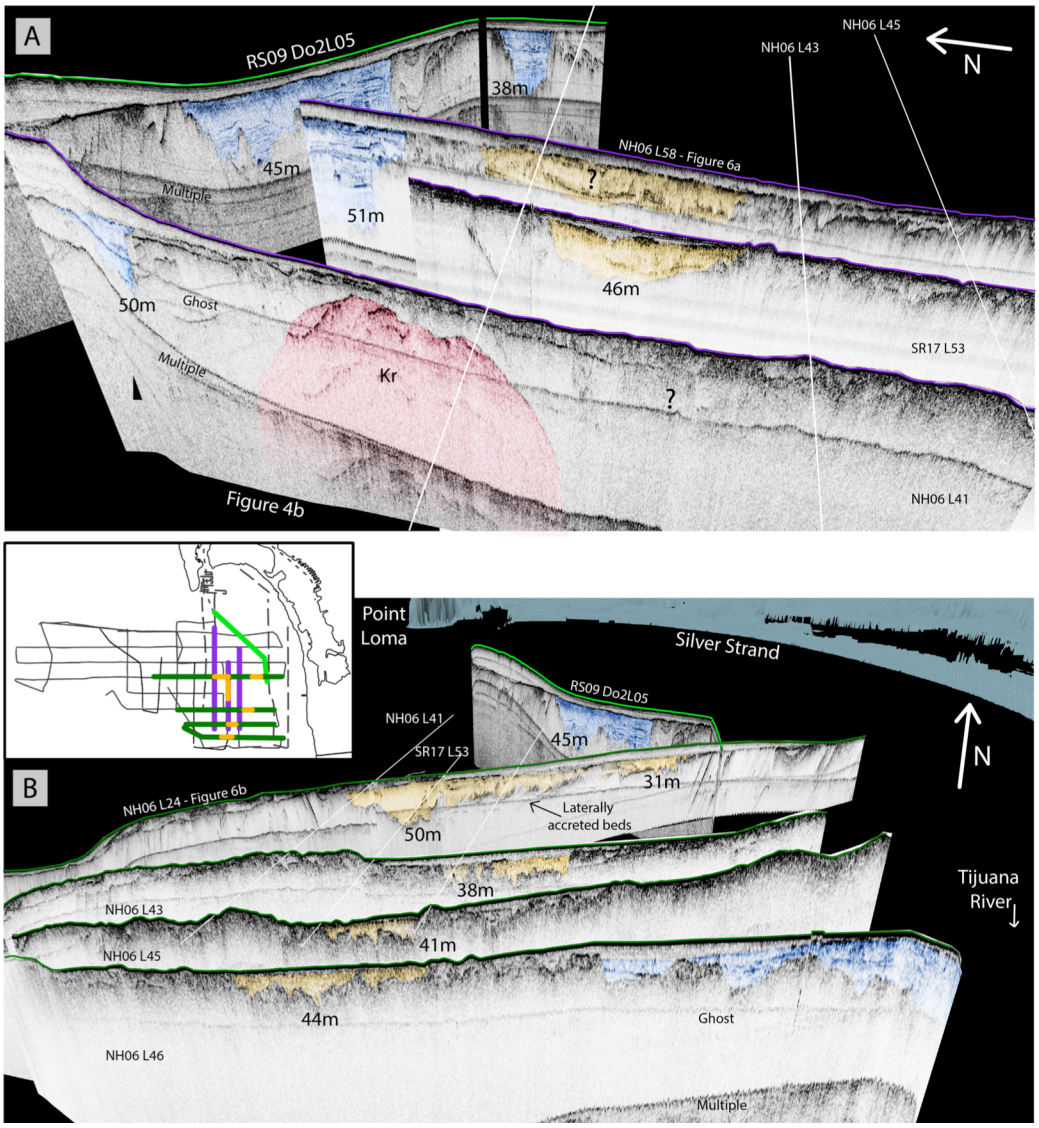

Figure 8. Seismic profiles arranged in 3D fence diagram to provide context for speculated paleochannel locations. The sea floor of profiles in each scene are traced in color corresponding to the inset map. The infill of speculated locations is highlighted in gold to allow for the reader's observation of the underlying surface. Interpreted channel locations are shaded with blue; The Cretaceous geology (Kr) is highlighted in red. White lines indicate location of intersecting profiles between the figures (i.e. white lines in Figure 8a show locations of lines in Figure 8b). (A) RS09-D02L05, D02L06 (green), and NH06-L41 (purple, forward), SR17-L53 (purple, middle), and NH06-L58 (purple, back, Figure 6a). View looking east at the possible channel component. (B) RS09- D02L05, D02L06 (green), NH06-L24, 43, 45, and 46 (from north to south). View looking north at possible southern components of the channel system.

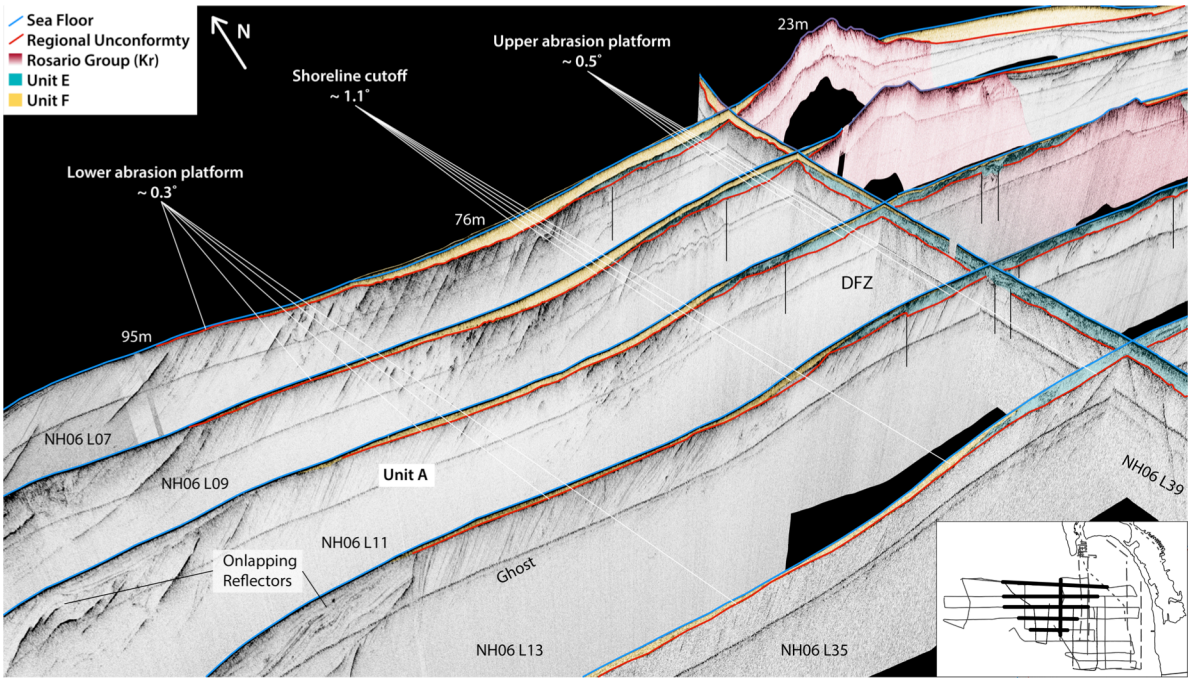

Figure 9. Lines NH06-L7, 9, 11, 13 and 35 intersected by L39, arranged in a fence diagram. Depths provided along NH06-L07 (back line). To the west (left) is the Loma Sea Valley and to the east (right) are the Silver Strand and San Diego Bay. Inset map shows location of lines in figure traced in thick black. Note location of Unit E is present over the upper (shallower) abrasion platform, east of the lower (deeper) abrasion platform, and west of the Cretaceous (Kr) sea floor outcrop, shaded in red. Descanso Fault Zone (DFZ) offsets are marked with black lines.

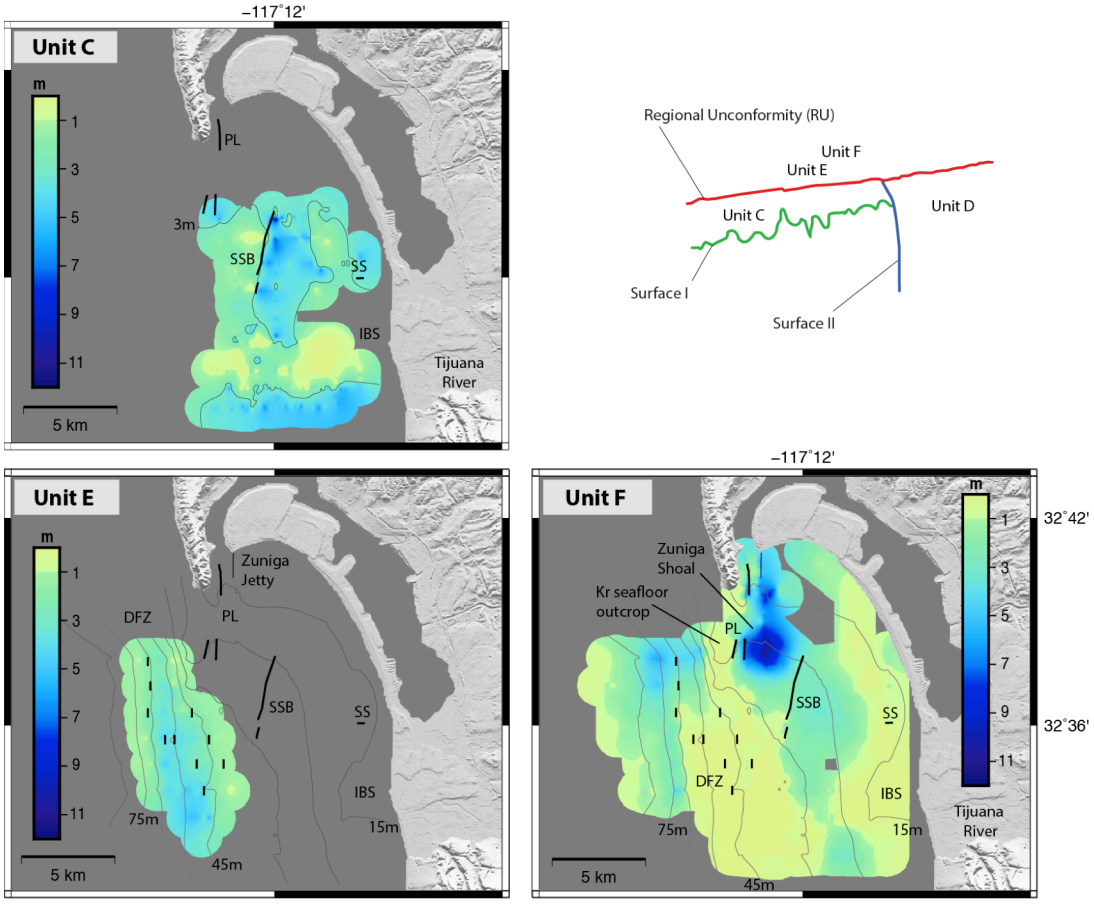

Figure 10. Isopach (thickness) maps of Unit C, E, and F. (A) Isopach (thickness) map of Unit C. PL = Point Loma Fault Zone; SSB = Southern Spanish Bight Fault; SS = Silver Strand Fault. IBS = Imperial Beach Shoal. (B) Schematic showing cross-cutting relationships of surfaces and the location of units C, D, E, and F above and between them. (C) Isopach map of Unit E, overlain with contours from the RU with 10m spacing. Unit E overlies the upper abrasion platform imaged in Figure 4. Faults observed in this study offsetting the RU are represented in thick black: DFZ = Descanso Fault Zone. (D) Isopach map of Unit F. The Zuniga shoal (dark blue area) has a thickness over 9m. Towards the west, Unit F thickens west of the Cretaceous seafloor outcrop (profiled by RU contour lines).

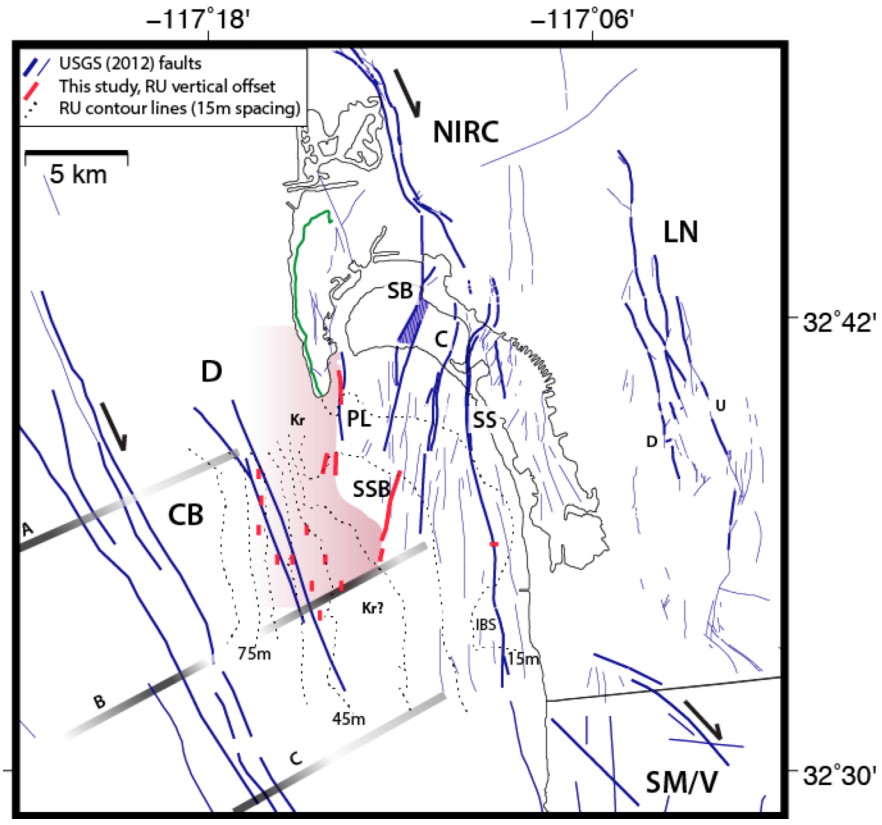

Figure 11. Fault map of the study area. Eastern extent of observed subsurface Cretaceous geology (Kr) shaded in magenta. Faults observed in this study that extend up to or offset the Regional Unconformity (RU) are colored red. RU contour lines are overlain in dashed black at 10m intervals. Shaded lines in the left corner represent location of MCS lines analyzed by Maloney (2013), where white represents basin depocenter and black represents regions where hardgrounds are exposed on the seafloor (see Figure 14). Dark blue hachured pattern on Coronado Island represents location of the now filled Spanish Bight. Green outline traces the MIS 5e Nestor Terrace observed between ~22-24 m above sea level. IBS = Imperial Beach Shoal. U/D shows relative fault offset. CB = Coronado Bank Fault Zone; D = Descanso Fault Zone; SSB = Southern Spanish Bight Fault; PL = Point Loma Fault Zone; SB = Spanish Bight Fault; C = Coronado Fault; SS = Silver Strand Fault; NIRC = Newport Inglewood/Rose Canyon Fault Zone; LN = La Nacion Fault Zone. SM/V = San Miguel/Vallecitos Fault Zone.

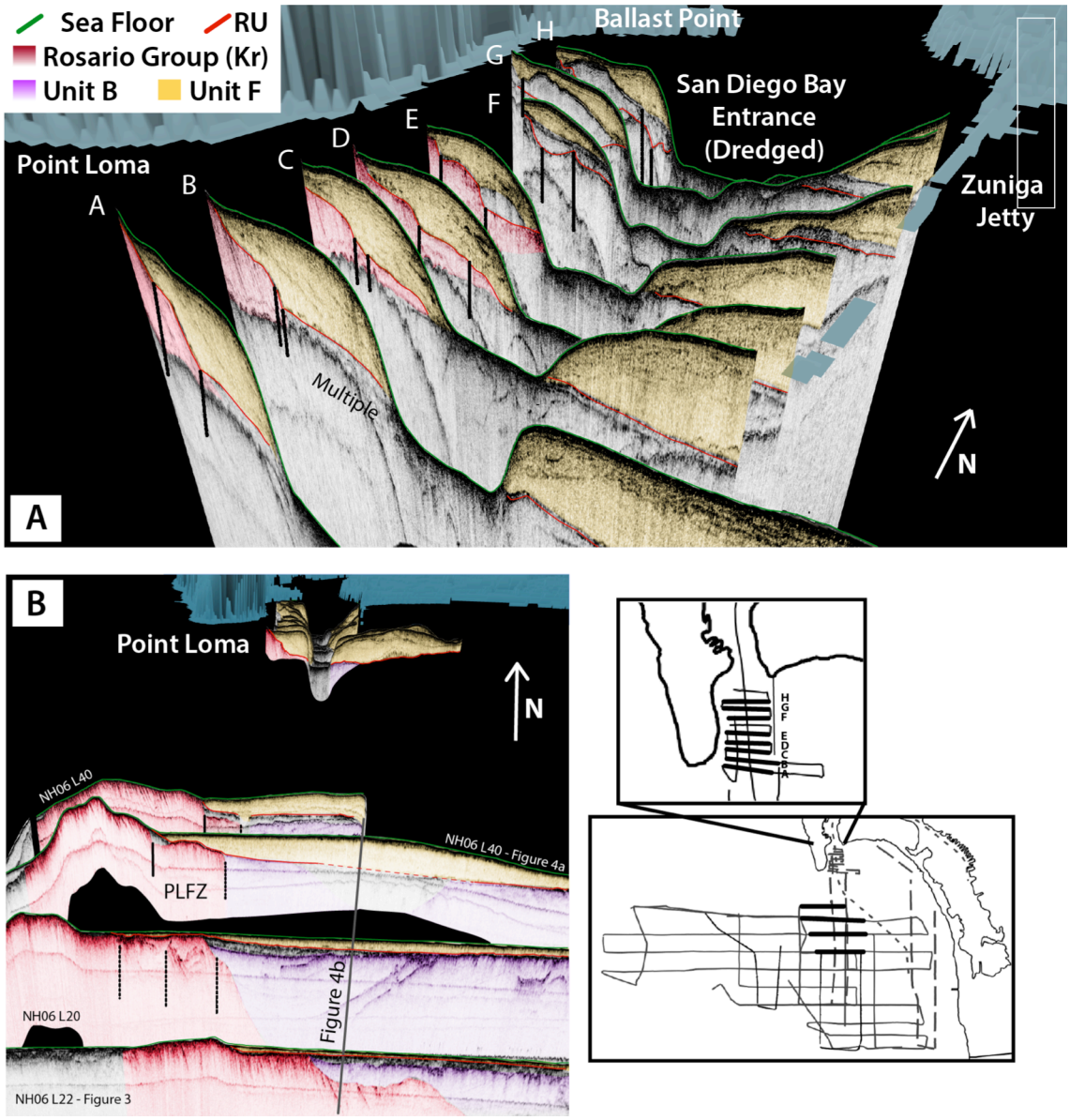

Figure 12. (A) PL15-D01L18, 16, 14, 3, 5, 7, 9, 11 (north to south). View looking northwest towards Point Loma, across the San Diego Bay Entrance. Observations of fault offset are traced with black lines. Maps show location of Figure 12a (zoomed map) and Figure 12b. (B) NH06-L40, 18, 20 and 22 (north to south), in addition to profiles from 12a. View looking north towards the bay entrance. Interpreted faults of the Point Loma Fault Zone (PLFZ) traced in black.

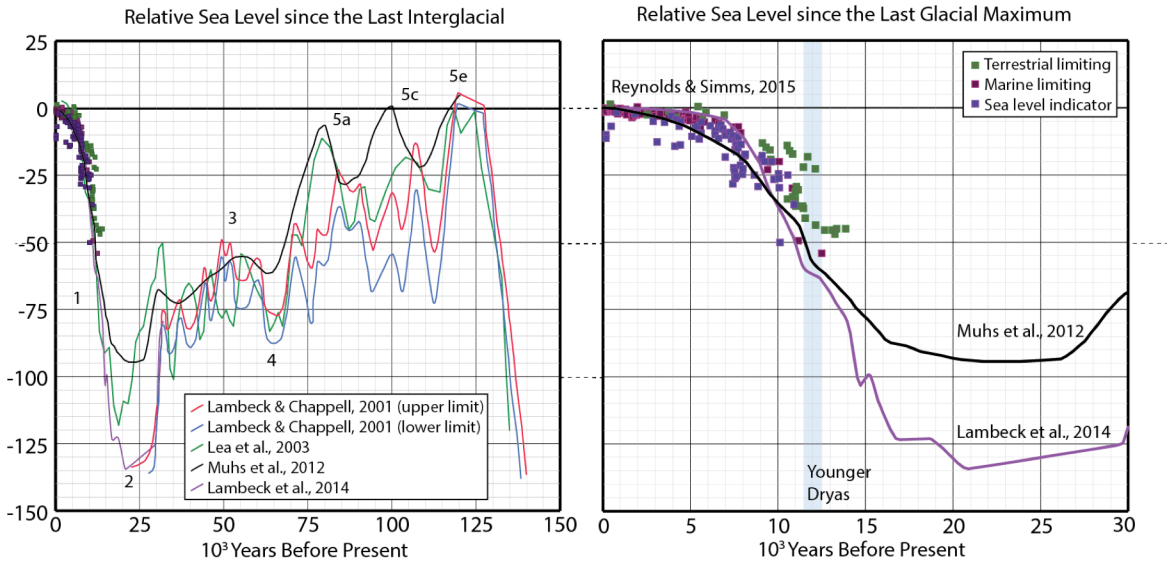

Figure 13. Sea level curves and data referenced in this study. (A) Sea level since the last interglacial (MIS 5, ~125 kya): In green is the benthic oxygen isotope curve from Lea et al. (2003); Traced in red and blue are the maximum and minimum sea level curves from Lambeck and Chappell (2001), respectively; The purple line represents data from Lambeck et al., (2014); Black traces the modeled, local sea level curve presented by Muhs et al. (2012), which matches uplift of observed marine terraces on San Nicholas Island. (B) Sea level since the Last Glacial Maximum (MIS 2, ~20 kya): Muhs et al. (2012) in black is continued from the inset; The purple line represents data from Lambeck et al. (2014); Scattered points are physical sea level indicators from Reynolds & Simms (2015): Green represents terrestrial limiting data; Purple represents marine limiting data; Magenta marks sea level indicating data. All curves account for Glacial Isostatic Adjustment (GIA) with the exception of Lea et al. (2003). Blue shaded column corresponds to the relative sea level still stand of the Younger Dryas, between ~12.5-11.5 kya.

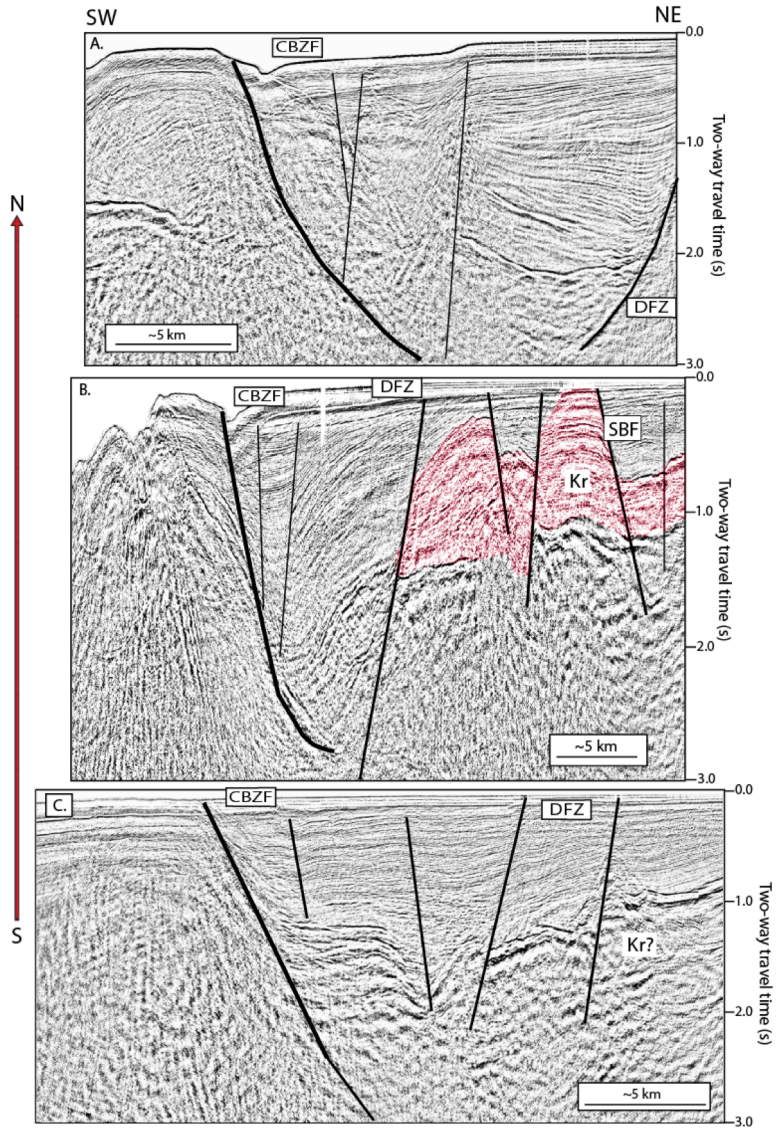

Figure 14. Multichannel Seismic lines interpreted by Maloney (2013). Extensional rollover on the Coronado Bank Fault Zone (CBFZ) observed to the west and normal, west dipping faulting along the western Descanso Fault Zone (DFZ). Red shading indicates interpreted location of Cretaceous geology (Kr = Rosario Group; See Figure 11 for line locations on map).